Stony Brook University

Laser Processing of Carbon Nanotube Transparent Conducting Films

A Thesis Presented

by

Andrew Mann

to

The Graduate School

in Partial Fulfillment of the

Requirements

for the Degree of

Master of Science

in

Mechanical Engineering

Stony Brook University

August 2013

Stony Brook University

The Graduate School

Andrew Mann

We, the thesis committee for the above candidate for the

Master of Science degree, hereby recommend

acceptance of this thesis.

Dr. David Hwang – Thesis Advisor
Assistant Professor, Mechanical Engineering

Dr. Jon Longtin – Second Reader
Associate Professor, Mechanical Engineering

Dr. Maen Alkhader – Third Reader
Assistant Professor, Mechanical Engineering

This thesis is accepted by the Graduate School

Charles Taber
Interim Dean of the Graduate School

Abstract of the Thesis

Laser Processing of Carbon Nanotube Transparent Conducting Films

by

Andrew Mann

Master of Science

in

Mechanical Engineering

Stony Brook University

2013

Transparent conducting films, or TCFs, are 2D electrical conductors with the ability to transmit light. Because of this, they are used in many popular electronics including smart phones, tablets, solar panels, and televisions. The most common material used as a TCF is indium tin oxide, or ITO. Although ITO has great electrical and optical characteristics, it is expensive, brittle, and difficult to pattern. These limitations have led researchers toward other materials for the next generation of displays and touch panels.

The most promising material for next generation TCFs is carbon nanotubes, or CNTs. CNTs are cylindrical tubes of carbon no more than a few atoms thick. They have different electrical and optical properties depending on their atomic structure, and are extremely strong. As an electrode, they conduct electricity through an array of randomly dispersed tubes. The array is highly transparent because of gaps between the tubes, and size and optical properties of the CNTs. Many research groups have tried making CNT TCFs with opto-electric properties similar to ITO but have difficultly achieving high conductivity. This is partly attributed to impurities from fabrication and a mix of different tube types, but is mainly caused by low junction conductivity.

In functionalized nanotubes, junction conductivity is impaired by covalently bonded molecules added to the sidewalls of the tubes. The addition of this molecule, known as functionalization, is designed to facilitate CNT dispersion in a solvent by adding properties of the molecule to the CNTs. While necessary for a good solution, functionalization decreases the conductivity in the CNT array by creating defects in the tube's structures and preventing direct inter-carbon bonding. This research investigates removing the functional coating (after tube deposition) by laser processing.

Laser light is able to preferentially heat the CNTs because of their optical and electrical properties. Through local conduction, the relatively weak functional molecules are thermally decomposed. This restores the pristine CNT structure and allows carbon to carbon bonds to form; thereby significantly improving the junction and sheet conductivity. Laser processing is performed without damaging the TCF substrate (usually glass or PET) because laser light is not absorbed by the substrate and conduction from the CNTs is limited.

In addition to removing the functional coating, laser light improves the electrical conductivity by purifying the CNT array. The purity is improved through the ablation of defective tubes and amorphous carbon in the CNT film.[1] Using higher laser power, it is possible to locally remove the CNTs. Selective laser removal of the CNTs is a dry process that can be used to pattern the electrode. This is a much simpler and less expensive patterning technique than wet acid etching used for ITO.

In summary, laser processing of CNT TCFs is shown to improve the electrical conductivity by defunctionalizing the CNTs. In addition, laser exposure increases purity by removing defects and can be used to pattern the electrode. These advances make CNTs more competitive as an alternative for ITO which has both cost and performance limitations.

TABLE OF CONTENTS

LIST OF FIGURES

LIST OF TABLES

ACKNOWLEDGMENTS

I dedicate this work to my family and friends for their continual support and to the memory of my sister Chelsea.

I would like to thank my advisor, Dr. Hwang, for his help and guidance over the last year. I would also like to thank Pyung-cho Han for his close collaboration with the experiments, Di Liu and Tao Zang for the SEM images and their help in the lab, Charles Wilhelm for his assistance with the experimental plan, and Hwan Lee for his help with the Raman spectroscopy.

I would like to thank Dr. Longtin and Dr. Alkhader for their support and for being on my thesis committee.

I would like to thank Stony Brook University and the Advanced Energy Research and Technology Center for the funding and lab space used for this research. And I would like to thank Brookhaven National Labs and Yuco Optics for the use of their equipment.

1. INTRODUCTION

Transparent conducting films, or TCFs, are thin two-dimensional electrical conductors that are used in many electrical devices including touch screens, LCDs, OLEDs, and solar cells. The increased demand and variety of these products pose difficulties for the traditional TCF material, indium tin oxide, or ITO. Fortunately, advances in nanotechnology have led scientists to develop transparent electrodes made of various nanomaterials. Of these, carbon nanotubes, or CNTs, are particularly promising but refinement in their use as a TCF is needed. This research investigates the effect of laser processing on the optoelectronic properties of CNT TCFs.

Currently, the most common TCF material is ITO, a metal oxide solution of indium(III) oxide and tin(IV) oxide at a 9:1 ratio. Its widespread use is primarily the result of its great opto-electric properties; less than 15 Ω/sq at 85% transmittance.[2] However this performance comes at a high price because of the scarcity of indium, a rare metal. As a ceramic, ITO is brittle which makes it difficult to process, implausible for flexible applications, and vulnerable to fracture. Additionally, its high index of refraction, ~2, and yellow hue lead to unwanted glare and screen color distortion. These drawbacks make ITO a poor solution for the growing performance and supply demand of the TCF industry.

An alternate transparent electrode material and the subject of a lot of ongoing research is CNTs. CNTs are one dimensional cylindrical carbon nanostructures approximately 1 nanometer in diameter and up to 18.5 centimeters long.[3] They consists of one or more layers of single-carbon-thick tubes. CNT's have different properties depending on the number of layers and atomic structure. The most significant example of this is their ability to conduct electricity like a metallic or semiconducting material. Metallic tubes are reported to have excellent mobility, ~10^5 cm^2/Vs,[4] and current carrying capacity, ~10^9 A/cm^2.[5] In general, CNTs are extremely strong; possessing a tensile strength as high as 63 gigapascals and a Young's moduli up to 950 gigapascals.[6] These properties make CNTs a good material for TCFs. Another advantage of CNTs is their ability to be made into solutions.

The benefit to having CNT solutions is the numerous easy deposition methods that can be used to make electrodes. The challenge lies in creating the solutions, because pure CNTs are not soluble in water and tend to group together into cords, known as bundling. There are three methods of creating CNT solutions; the first uses neat organic solvents or super acids to dissolve the CNTs. The second method involves solubilization agents such as surfactants and dispersants that prevent bundling and aid dissolution. The third method, known as functionalization, uses a covalently bonded molecule on the surface of the CNTs to prevent bundling and help dissolution. Once the CNTs are in solution form, they can be added to a substrate by vacuum filter, Mayer bar, roll-to-roll, spin, dip, or spray coating. These wet deposition methods are much easier to use than their dry alternatives, e.g. sputter deposition of ITO. The CNT TCFs studied in this report were spray coated using functionalized CNTs.

Electrodes made from CNTs conduct electricity through a 2D network of randomly distributed overlapping tubes. The excellent mechanical and electrical properties of the individual tubes make the CNT array strong and conductive. Optically, CNT networks can be highly transparent depending on the amount of space between tubes, called the void fraction, and the film thickness. In addition, they are color neutral and have a low index of refraction, ~1.5.[7] Compared to ITO, CNT TCFs are mechanically and optically superior, and cheaper and easier to produce. However, CNT thin film networks typically have a sheet resistance several orders of magnitude higher than that of ITO at the same transmittance. Poor electrical conductivity is the result of impurities from fabrication, a mix of different tube types including semiconducting tubes, and low junction conductivity.

For functionalized CNTs, the poor electrical connection between tubes is the result of the covalently bonded molecule attached to the sidewalls. This coating, designed to minimize bundling in solution, damages the carbon sp^2 bonds and prevents the good inter-tube electrical connections. This research shows improvement of the electrode conductivity through laser removal of the functional molecules. Laser irradiation preferentially heats the CNTs and, through local conduction, thermally decomposes the functional group. Once defunctionalized, the CNTs recover their high electrical conductivity and form better electrical connections to tubes in close proximity. Laser heating, rather than ordinary conduction heating, is used because it is able to heat the CNTs to high temperatures without damaging the substrate. This is possible because the substrate, usually glass or PET, is transparent to the laser beam and the thermal diffusion length from the heated tubes is significantly less than the substrate thickness.

In addition to improving the junction conductivity, laser processing can be used purify and pattern the electrode. Laser irradiation has been shown to be effective at removing impurities, amorphous carbon, and defective CNTs.[1] Laser ablation of these impurities happens at a lower power than removal the CNTs because they have weaker bond energy than sp2 bonded CNTs. Higher power laser irradiation can be used to selectively remove the CNTs. This is a dry processing method that can be used to pattern the electrodes for applications including touch screens and displays. Dry processing is cheaper and less hazardous than wet alternatives, such as chemical etching of ITO.

Laser processing can be used to improve junction conductivity, purify, and pattern a CNT TCF. This research shows that removal of the molecules bonded to functionalized CNTs lowers the sheet resistance of the electrode. Laser heat transfer was used because it locally heats the CNTs to high temperatures without damaging the substrate. Improvement of the electrical conductivity is necessary if CNTs are going to replace ITO as the most common TCF material.

Chapter 2 provides an introduction to CNTs. The atomic and electrical structure of single walled CNTs is examined. A characterization of the electrical, optical, and mechanical properties of CNTs is presented. And the three primary synthesis methods, arc-discharge, laser ablation, and chemical vapor deposition, are discussed.

Chapter 3 provides more information about CNT solutions, CNT TCFs, and the samples used in this report. The three types of CNT solutions briefly mentioned above and the numerous wet coating methods are defined in greater detail. The properties of CNT TCFs that have been observed in other research are presented. And an in depth characterization of the samples used in this report is made.

Chapter 4 delves into laser processing of CNTs, focusing on removal of the functional molecule but also discussing laser patterning and purification. A brief introduction to lasers is presented. The difficulty of modeling CNT absorption and reflection of laser light is discussed. The ultimate effects of laser irradiation are described. And the advantages, disadvantages, and limitations of laser processing are mentioned.

Chapter 5 discusses the methods used to evaluate the CNT TCFs and presents descriptions of the experiments along with the results. The evaluation methods include two and four-wire resistance measurements, optical and SEM imaging, and Raman spectroscopy. The experiments mainly investigate the effects of increased laser irradiation on the sample conductivity. Also included are experiments on electrode stability and homogeneity.

Chapter 6 is a discussion of the results highlighting the change in electrical and optical characteristics and also including comments about the mechanical properties. A comparison between these experiments results, other published CNT electrode properties, and ITO TCFs available to industry is made.

Chapter 7 presents the next steps that should be taken in investigating and improving CNT TCFs. This includes a quantitative analysis of the optical properties, investigating the mechanical-electrical relationship, and creating samples from higher purity metallic tubes.

Chapter 8 provides a brief overview of the research conducted emphasizing the success and potential significance of the work.

2. CARBON NANOTUBE INTRODUCTION

Carbon nanotubes, or CNTs, are single-atom-thick tubes of carbon with diameters approximately 50,000 times smaller than that of a human hair. They were first discovered in 1952 by Russian scientists L. V. Radushkevich and V. M. Lukyanovich using transmission electron microscopy (TEM).[8] CNTs received little attention until the 1990's and are currently one of the most popular research subjects. There are many different types of CNTs and their exceptional properties make them interesting to a wide range of fields.

2.1. CNT STRUCTURE

2.1.1. Atomic Structure. The structure of a carbon nanotube can be envisioned as a single layer of graphite, known as graphene, rolled into a cylinder. Graphene is a 2D plane of sp^2 bonded carbon with a honeycombed structure and a thickness of one atom. Different types of CNTs exist depending on the "chiral" angle at which the graphene is wrapped. This angle is related to the chiral vector, $\vec{C}_h$, a vector that points along the circumference of the tube. The chiral vector is defined by the unit vectors, $\hat{a}_1$ and $\hat{a}_2$, using a pair of indices n and m.

$$\vec{C}_h = n\hat{a}_1 + m\hat{a}_2 \tag{2.1}$$

The vectors $\hat{a}_1$ and $\hat{a}_2$ are created by connecting the first and third, and first and fifth carbon atoms in a single honeycomb structure. The angle between them is 60°. Figure 2.1(a) shows the chiral vector and unit vectors $\hat{a}_1$ and $\hat{a}_2$. The length of the unit vectors is $a_{1,2} = \sqrt{3}a_{C-C}$ where $a_{C-C} = 1.42$ Å, the length of the C-C bond.

The chiral vector is important because it can be used to directly solve for the diameter and chirality of a CNT. The tube diameter is equal to the length of the chiral vector divided by π. And the chirality is defined by the chiral angle, θ_{ch}, measured between $\vec{C}_h$ and $\hat{a}_1$.

$$d_{CNT} = \frac{|\vec{C}_h|}{\pi} = \frac{\sqrt{3}a_{C-C}}{\pi}\sqrt{n^2 + nm + m^2} \tag{2.1}$$

$$\theta_{ch} = \arctan\left(\frac{m\sqrt{3}}{2n + m}\right) \tag{2.1}$$

Since the chiral vector only depends on n and m, CNTs are usually classified by their (n, m) index, some of which have special names. Tubes with $m = 0$ ($\theta_{ch} = 0$) are called zigzag, and $n = m$ ($\theta_{ch} = 30°$) are called armchair. All other tubes ($0 < \theta_{ch} < 30°$) are referred to as chiral. Figure 2.1(b) shows the carbon structure for an armchair, zigzag, and chiral CNT.

In addition to different chiral angles, CNTs can have more than one layer of carbon atoms. There are two types of layering schemes. In the Russian doll model, the layers are concentric cylinders, i.e. large diameter CNTs surrounding smaller diameter CNTs. In the parchment model, a single sheet of graphene in rolled around itself like a piece of paper.

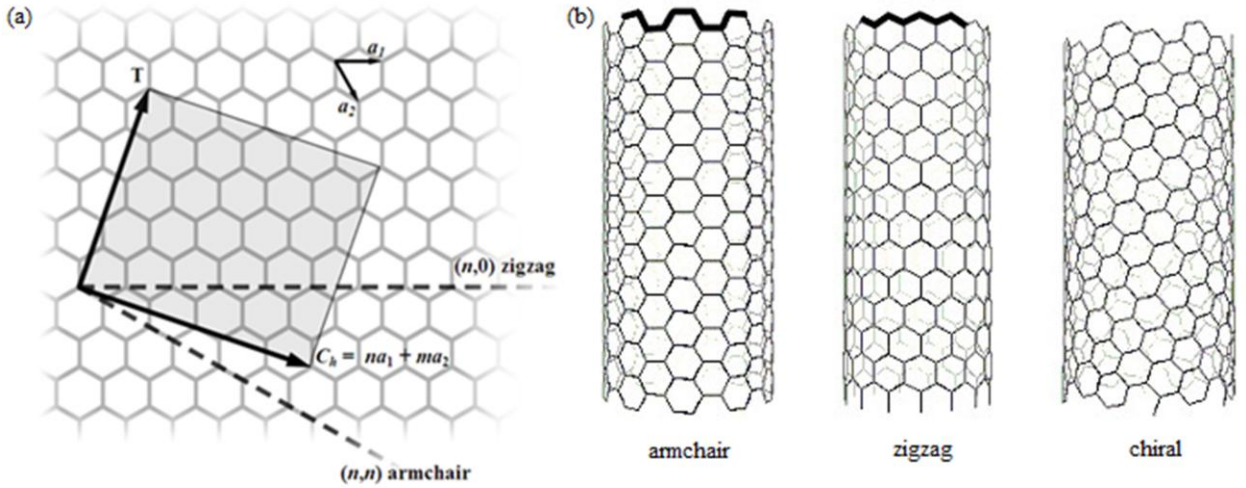

Figure 2.1. (a) A sheet of graphene with vectors showing the (***n***, ***m***) CNT naming index.[9] (b) Examples of an armchair, zigzag, and chiral SWNT.[10]

Parchment type tubes are less common so Russian doll tubes should be assumed unless otherwise stated. CNTs are separated into three categories; single-wall carbon nanotubes (SWNTs), double-wall carbon nanotubes (DWNTs), or multi-wall carbon nanotubes (MWNTs). The term MWNTs is often used in a general sense that includes DWNTs.

2.1.2. Electronic Band Structure. It is important to classify a CNT by its (n, m) index because the atomic structure has a strong effect on the electronic band structure. The electronic band structure is the composition of all the energy levels that an electron may occupy in a material. The band structure of CNTs is similar to that of graphene but varies due to the periodic boundary condition created by the seamless wrapping of the carbon lattice. Graphene's band structure is made up of four valance electrons from each carbon atom. Three of these participate

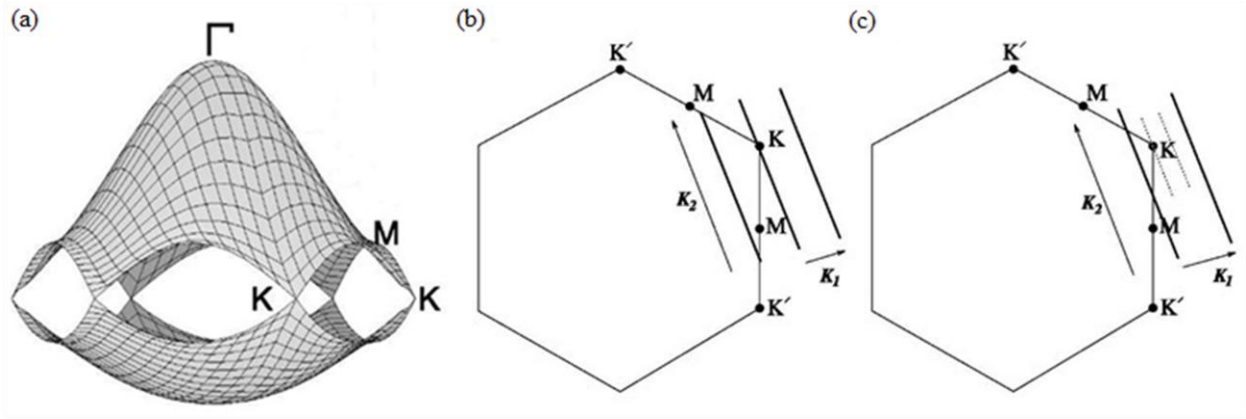

Figure 2.2. (a) The energy dispersion relation for graphene shown within the 3D Brillouin zone. The upper and lower surfaces represent the conduction (***π****) and valance (***π***) bands. [11] Plots of the *k*-vectors in the 2D Brillouin zone near the K point for (b) a semimetallic and (c) a semiconducting CNT.[11]

in the sp^2 bonds with the surrounding atoms and belong to the σ valance band and σ^* conduction band. The fourth valance electron forms the π and π^* valance and conduction bands. The electronic behavior of graphene is the result of an occupied π band and an unoccupied π^* band near the Fermi energy. These two bands meet at the Fermi level at the *K* points in the Brillouin zone, as shown in figure 2.2(a), making graphene a zero-gap semiconductor, or semimetal.

Unlike graphene, CNTs can be metallic, semimetallic, or semiconducting. For CNTs, a periodic boundary condition exists in the circumferential direction owing to the wrapping of the tube along the chiral vector. As a result, the *k*-vectors associated with the circumferential direction are limited to a finite number of solutions. The permissible *k*-vectors, plotted as lines in figure 2.2(b-c), depend on the chiral vector of the tube. A CNT with a *k*-vector that passes through adjacent K and K' points in the Brillouin zone is degenerate at the Fermi energy and is therefore metallic. CNTs with a *k*-vector passing through only one K point have zero bandgap and are semimetallic. And CNTs with *k*-vectors that do not pass through either point have a small bandgap and are semiconducting.

The (n, m) index can be used to determine if a CNT is metallic, semimetallic, or semiconducting. All armchair, $n = m$, tubes are metallic. Tubes that satisfy $(n - m) = 3i$, where i is a nonzero integer, are semimetallic. And all other tubes are semiconductors. These relationships can be confirmed by looking at the band structure of each type of CNT near the

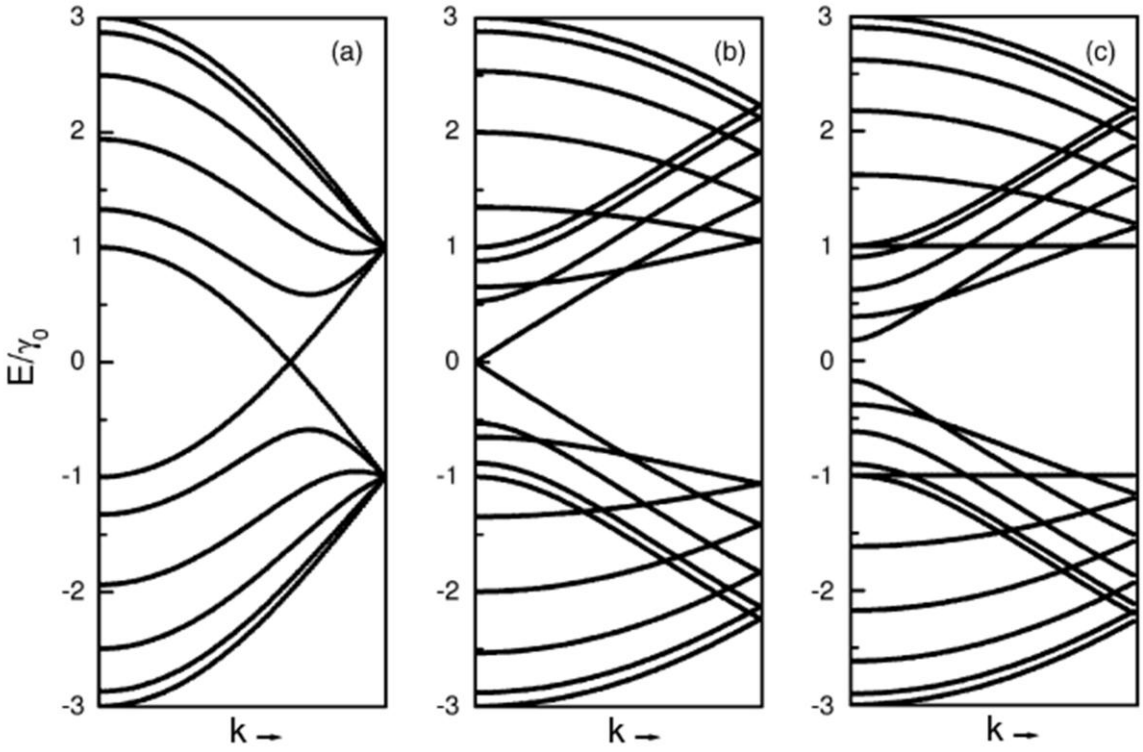

Figure 2.3. The electronic band structures for a (a) metallic armchair (5, 5), (b) semimetallic zig-zag (9, 0), (c) and semiconducting zig-zag (10, 0) CNT.[12]

Fermi energy. Metallic tubes show overlapping π and π^* bands, shown in Figure 2.3(a). Semimetallic tubes have a band structure similar to graphene with the π and π^* bands touching at the Fermi energy, figure 2.3(b). And semiconducting tubes show a small gap between the π and π^* bands, figure 2.3(c).

2.1.3. Density of States (DOS). Closely related to the band structure is the density of states, or DOS. The DOS is the number of quantum states that can be occupied within a given energy level. Unlike a three dimensional material, the DOS of a CNT is discontinuous; that is, sharp peaks, known as Van Hove singularities, exist in the number of available electron states. Van Hove singularities in CNTs are caused by flat regions in the energy dispersion relation. Near the Fermi energy, the DOS is constant because the energy dispersion relation is linear. Like the band structure, the DOS of a CNT is dependent on chirality and diameter, as shown in Figure 2.4(a). Metallic tubes have a non-zero DOS near and at the Fermi energy that is inversely proportional to the tubes diameter. The DOS for semimetallic tubes is non-zero near the Fermi energy but drops to zero at the Fermi energy. Semiconducting tubes have a DOS of zero near and at the Fermi energy. The first singularities on either side of the Fermi energy represent the highest lying valence band and the lowest lying conduction band. The energy gap between them,

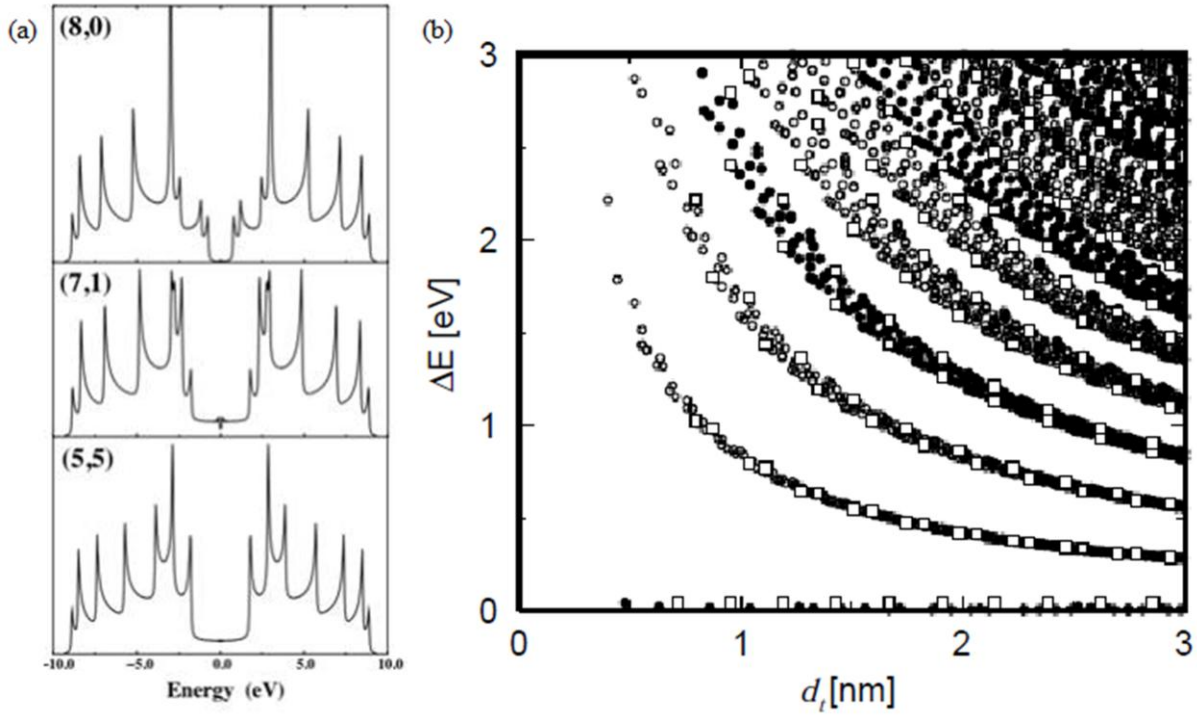

Figure 2.4. (a) The DOS for a semiconducting zig-zag (8, 0), semimetallic chiral (7, 1), and metallic armchair (5, 5) CNT.[#] (b) The energy difference between symmetrical Van Hove singularities in the DOS. Solid and unfilled circles correspond to metallic and semiconducting tubes, and squares correspond to zig-zag CNTs.[#]

and between subsequent singularity pairs, is inversely proportional to the tube diameter, as shown in Figure 2.4(b).

2.2. CNT PROPERTIES.

2.2.1. Electrical Transport. Electrical transport in CNTs is increasingly important as more and more ways to use CNTs in nanoelectronic devices are imagined. Recent work has led to CNT single-electron transistors, field effect transistors, and rectifying diodes. One of the leading reasons for interest in CNTs is their remarkable ability as a one-dimensional conductor. They are the only one-dimensional conductor that can operate at room temperature, have a strong mechanical structure, and are chemically inert. The electrical transport of a CNT at room temperature can be analyzed by applying a load voltage and measuring the corresponding current. The resulting I-V curve will be linear and invariant with gate voltage for metallic tubes. Semiconducting tubes show a strong dependence on gate voltage, see figure 2.5(a). Figure 2.5(a) shows that semiconducting CNTs are hole-doped, p-type semiconductors. For gate voltages less than one, the semiconducting CNT shows highly metallic behavior. As the Gate voltage increases, a large gap forms and the tube becomes highly insulating.

Metallic CNTs are predicted to have an ideal two terminal resistance of 6.5 kΩ. This is strongly supported by experimental measurements of as low as 10 kΩ for a single nanotube's resistance.[16] Additionally, it has been determined that CNTs have mobilities on the order of 10^5 cm^2/Vs, and current carrying capacities on the order of 10^9 A/cm^2.[24,25] The electrical transport behavior of CNTs is particularly interesting at extreme temperatures. At temperatures close to zero Kelvin, single-electron charging, resonant tunneling through discrete energy levels, and

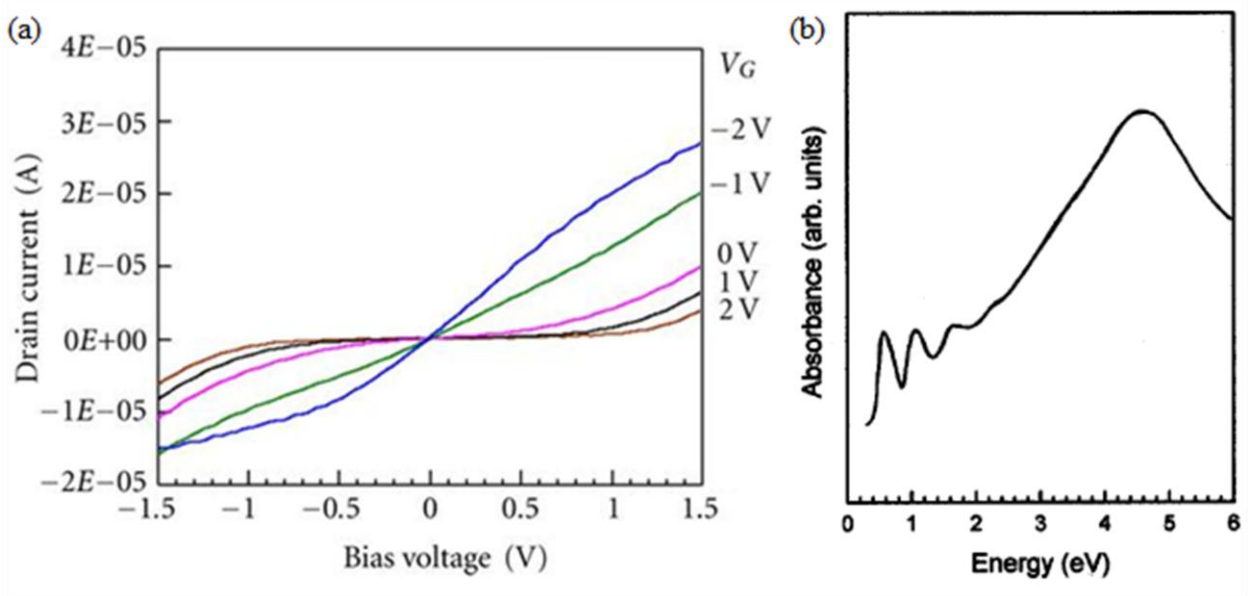

Figure 2.5. (a) The I-V curve for a hole doped, p-type semiconducting SWNT.[15] (b) The optical absorption spectrum of a thin film of SWNTs.[12]

proximity-induced superconductivity has been observed.[7] CNTs at high temperatures show one-dimensional Luttinger liquid mode tunneling conductance.

2.2.2. Optical Absorption. Optical absorption in carbon nanotubes is characterized by the electronic transitions between the symmetrically opposed Von Hove singularities near the Fermi energy in the DOS.[17] Unlike three-dimensional materials where there is an absorption threshold followed by a steady increase in absorption, the optical absorption spectrum of CNTs shows peaks that match up with the Van Hove singularities in the DOS, as seen in figure 2.5(b). The first two peaks, at ~0.6 eV and ~1.2 eV correspond to Van Hove singularities in semiconducting tubes. The third peak, at ~1.7 eV, corresponds to a Van Hove singularity in metallic tubes. The large absorption band at ~4.5 eV is attributed to π-plasmons in the CNT. A group of CNTs with the same chirality will absorb light at a preferred wavelength corresponding to the Van Hove singularities. Conversely, a collection of different CNTs will absorb light more like a solid because the peaks in the absorption spectrum will be mitigated by the combination of different spectrums.

2.2.3. Mechanical Strength and Stiffness. CNTs have an extremely high axial strength and stiffness owing to the strong sp^2 carbon bonds that make up their atomic structure. Tensile loading with an atomic force microscope (AFM) was used to examine the Young's modulus and tensile strength of a SWNT, see figure 2.5. Values between 11 and 63 GPa were measured for the Young's modulus and between 270 and 950 GPa for the tensile strength.[19] Despite their excellent properties is the axial direction, it has been determined that CNTs are rather weak in the radial direction. An AFM probe was used to deflect a CNT until it buckled at ~10° and a bending strength of about 14 GPa was measured.[20]

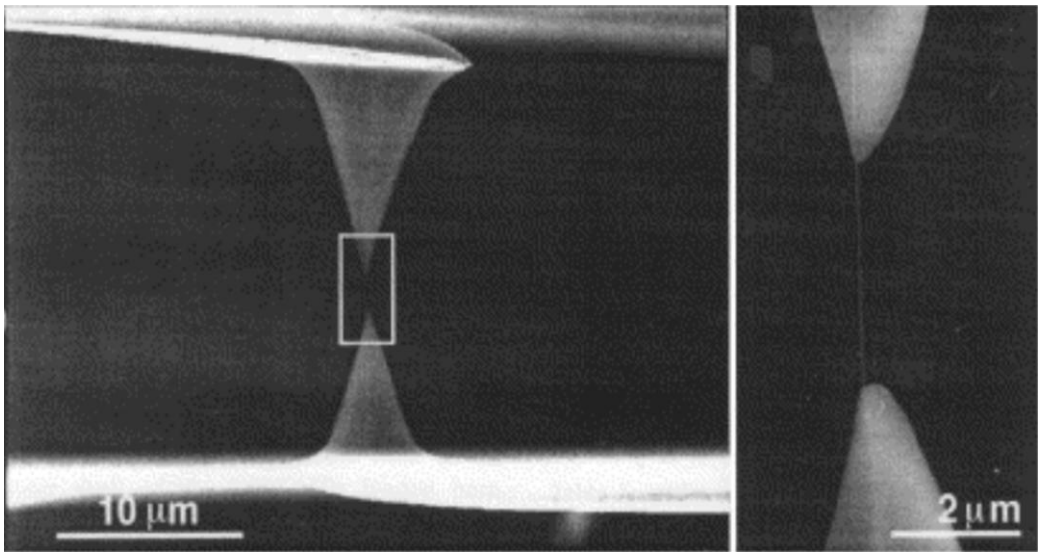

Figure 2.6. Scanning electron microscope (SEM) image of a SWNT under tensile loading.[18]

2.3. CNT SYNTHESIS

Synthesis is extremely important because most CNT applications call for a specific type of CNT, e.g. metallic, single wall, etc. It is extremely difficult to create nanotubes with uniform chirality, diameter, and number of walls. Minimizing the amount of impurities that are produced during fabrication is also a challenge. The three prevalent forms of CNT synthesis are arc-discharge, laser ablation, and chemical vapor deposition.

2.3.1. Arc-Discharge. Synthesis of CNTs by arc-discharge was inadvertently performed in 1991 during the production of fullerenes, a similar one-dimensional carbon structure.[8] Since then, arc-discharge has become a dominant method of CNT fabrication. Two carbon rods, an anode and a cathode, are placed approximately 1 millimeter apart in an inert liquid or gas. An arc discharge of 50 to 100 amps is created between the electrodes by an imposed potential difference.[21] The carbon on the cathode is vaporized by the high temperatures from the arc discharge and is deposited as CNTs on the anode. Arc-discharge method can be used to make both SWNTs and MWNTs but a metal catalyst is needed to fabricate SWNTs.

2.3.2. Laser Ablation. Like arc-discharge, laser ablation works by vaporizing carbon and allowing it to restructure into CNTs. Carbon rods containing a catalyst, typically a mix of nickel and cobalt, are place in a container with an inert gas at a high temperature (~1000°C). A pulsed laser is used to heat and vaporize the carbon, which then restructures into CNTs. This method primarily creates SWNTs and can achieve yields in excess of 70 weight percent.[21] Additionally, laser ablation can synthesis tubes with a specific diameter by varying process parameters.

2.3.3. Chemical Vapor Deposition. Chemical vapor deposition, or CVD, of CNTs was reported in the 1950's but CNTs were not produced using this method until 1993.[22,23] In the CVD process, a substrate containing catalytic metal particles is heated to high temperatures. Then a process gas (e.g. ammonia, nitrogen, or hydrogen) and a carbon containing gas (e.g. acetylene, ethylene, or ethanol) are mixed and the carbon containing gas is broken down. Carbon forms around the edge of the metal particles and grows into tubes. Depending on the catalyst, different diameter tubes can be grown. CVD is the most effective method for producing CNTs on a large scale because it is cheaper than arc-discharge or laser ablation.

3. CARBON NANOTUBE TRANSPARENT CONDUCTING FILMS (CNT TCF'S)

Of the many applications for CNTs, transparent conducting films, or TCFs, is one that will likely to make it into numerous consumer electronics. Among other things, TCFs are currently used in smart phones, tablets, and flat screen TVs. A CNT TCF works by conducting electricity through a two dimensional array tubes that is thin enough for light to pass through it. Figure 3.1(a) shows a flexible CNT TCF. The potential for CNT TCFs comes from the excellent properties of CNTs, and the advantageous fabrication methods of producing TCFs out of CNTs.

3.1. FABRICATION OF CNT TCFS

3.1.1. Dissolution and Dispersion. One advantage to using CNTs over other TCF materials is that CNTs can be forced into solution; Figure 3.1(b) shows a solution of CNTs in N-methyl-2-pyrrolidone. This makes it possible to use a number of simple wet deposition techniques when coating the substrate. Unfortunately, CNT's are not normally soluble in water because they exhibit a strong inter-tube attraction caused by the Van der Waals force. This attraction causes the tubes to group together into bundles and prevents their dissolution. As a result, various techniques have been developed to disperse CNTs, and make them into solutions. The three primary methods of creating CNT solutions use neat inorganic and superacid solvents, solubilizates, and functional groups to disperse and dissolve the tubes.

The use of neat inorganic and superacid solvents makes direct dissolution of the CNTs possible. This is by far the simplest method of creating CNT solutions. Additionally, it does not add impurities, such as solubilizates and functional groups, to the solution. Some common solvents capable of directly dissolving CNTs are dimethylformamide, N-methyl-2-pyrrolidone, chloroform, and dichlorobenzene.[16] The main issue with direct dissolution is obtaining solutions

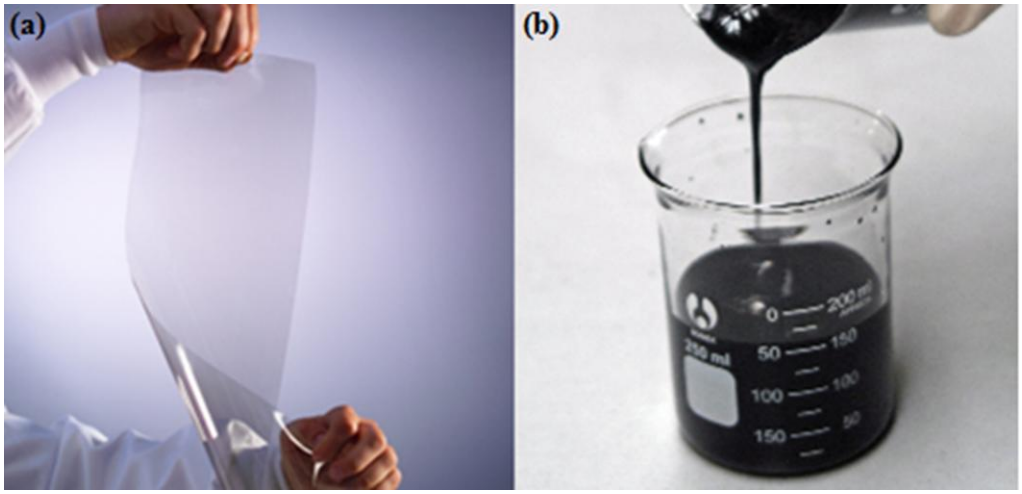

Figure 3.1. (a) A flexible CNT TCF.[27] (b) A solution of CNTs in NMP with a 5wt%.[28]

with a high enough concentration of CNTs. Most solvents cannot support more than 0.1 g/L, which makes them less useful in industrial applications.[16] Some solvents have been shown to directly dissolve CNTs at higher concentrations; however, drawbacks such as a high boiling point or high acidity make them impractical.

Solubilizates can be used to create CNT quasi-solutions, that is, colloids and suspensions. Unlike a solution, colloids and suspensions are heterogeneous mixtures that contain solid particles that are mechanically dispersed throughout the solvent. The difference between colloids and suspensions is that a colloid will never separate. In this report, the term solution refers to true solutions as well as colloids and suspensions. Solutions made using solubilizates can have a much higher concentration than would otherwise be possible. For CNT solutions, surface active agents known as surfactants are the most commonly used solubilizates. Surfactants absorb onto a CNT and decrease the interfacial tension between it and the liquid, thereby improving dispersion. They are particularly useful because they enable the solubilization of CNTs in water and other common solvents. A few common surfactants are Sodium dodecyl benzene sulfonate (SDBS), Sodium dodecyl sulfate (SDS), Lithium dodecyl sulfate (LDS), tetradecyl trimethyl ammonium bromide (TTAB), and Sodium cholate (SC).[16] The disadvantage of using solubilizates is that they are deposited onto the substrate along with the CNTs and usually have a negative effect on performance.

Similar to adding surfactants, adding functional groups to the CNT makes them disperse better in a solvent. CNT functionalization is the covalent bonding of molecules to some of the tube's carbon atoms. These molecules add some of their characteristics, or "functions", to the CNT. Functionalization is achieved by breaking some of the sp^2 carbon bonds, via oxidation and ultrasonication, in a mixture of nitric and sulfuric acid.[24] As a result, functional oxygen containing molecules are added to the tubes. These molecules, mainly from the carboxyl group, attach to the ends and sidewalls, as shown in Figure 3.2. Other functional groups are sometimes created by modifying and adding to the carboxyl functionalization. Common functional chains include OH, COOH, O+, CO, and NH_2. Each of these uses a different method to disperse and

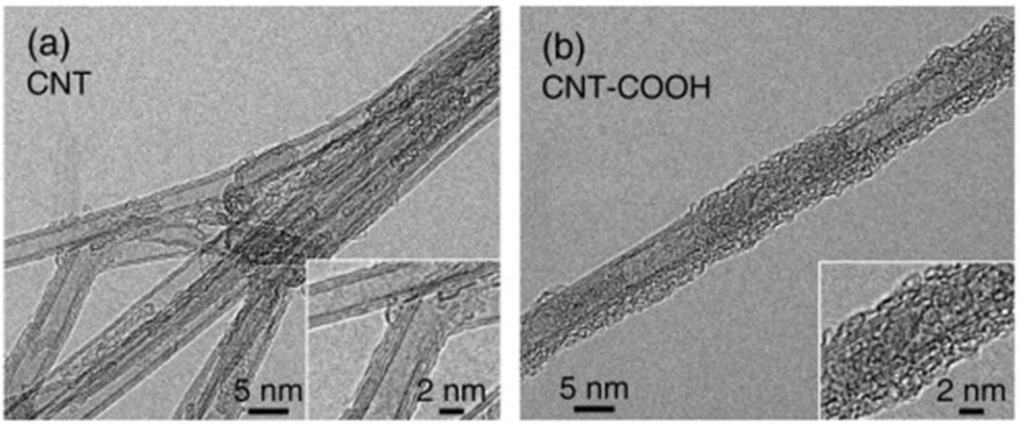

Figure 3.2. Transmission electron microscope (TEM) images of a (a) non-functionalized CNT, (b) and a COOH functionalized CNT.[29]

dissolve the tubes. Carboxyl functionalized CNTs form suspensions in solvents with a pH below 8. Ionization of the carboxyl group facilitates dispersion between the electrically charged COO- chains.[26] Conversely, tubes functionalized with azomethine ylide are soluble in organic solvents and water. Concentrations as high as 50 g/L in $CHCl_3$ are possible.[24] The main problem in using functionalized CNTs is that the damage done to the sp^2 bonds decreases structural and electrical integrity of the nanotubes. However, this damage can be reversed by thermally annealing the CNTs, see section 3.1.3.

3.1.2. Substrate Coating. Having a solution containing CNTs makes it much easier to fabricate films with a uniform coating quickly. There are many so-called "wet" substrate coating methods, including vacuum filtration, ink jet printing, Mayer bar coating, roll-to-roll coating, spin coating, dip coating, and spray coating. These methods are far simpler, cheaper, and more effective than dry coating alternatives, such as the sputter deposition of ITO. Table 3.1 provides a short description of each method and indicates the associated film quality and production scale. Roll-to-roll coating is by far the most effective coating method for industrial scale production but is typical too expensive of a setup for a laboratory. Spin, dip, and spray coating methods are commonly used for small scale laboratory production because they are simple and cheap. Additionally, dip and spray coating methods can be used to deposit tubes on contoured surfaces. Vacuum filtration and Mayer bar coating are used to make electrodes with good film uniformity on a small scale. Vacuum filtration is particularly popular because it works well with dilute solutions and can be used to rinse out surfactants. Electrodes often require some post-deposition subtractive patterning; ink jet printing is useful because it is able to deposit CNTs in patterns.

Table 3.1. A description and evaluation of the various wet coating methods used to make CNT TCFs.

Coating Method	Description	Film Uniformity	Production Scale
Vacuum filtration	A CNT solution is drawn through a porous membrane with a vacuum, then the deposited tubes are transferred to a substrate	Good	Small
Mayer bar coating	A CNT solution is drawn over a substrate using a metal bar wrapped in wire	Good	Small
Roll-to-roll coating	A CNT solution passes between two cylinders and is deposited to a moving substrate.	Good	Large
Spin coating	A substrate with a small amount of CNT solution at its center is spun at high speeds	Poor	Small
Dip coating	A substrate is submerged and slowly drawn from a CNT solution	Poor	Small
Spray coating	A CNT solution is sprayed onto a substrate using an air brush	Poor	Small
Ink jet printing	A CNT solution is deposited on a substrate using an ink jet printer	Good	Moderate

3.1.3. Heat Treatment. Thermal annealing can be used during or after the deposition process to improve the uniformity and performance of the electrode. One issue with wet processing of CNTs is that convection patterns within the evaporating solvent lead to a non-uniform deposition of CNTs. This is a significant problem during spray coating where CNTs are deposited in rings due to the coffee stain effect. This effect can be countered by accelerating evaporation through the use of volatile solvents or heat treatment during deposition. For other coating methods, heating of the substrate after deposition is commonly practiced to speed up evaporation. Heat treatment is also used to improve the electrical and mechanical properties of functionalized CNTs. It has been shown that thermal annealing can remove functional groups without damaging CNTs; annealed CNTs recover their original pristine nanotube properties.[30] Optimal recovery is achieved at temperatures greater than 400°C.[30] Chapter 4 discussed the use of lasers for thermal annealing.

3.2. CNT TCF PROPERTIES

3.2.1. Electrical Properties. The electrical properties of CNT TCFs are the result of electrons flowing through a network of thousands of tubes. The electrical conductivity of the network is primarily the result of highly resistive tube junctions. A single metallic tube has a resistance of approximately 10 kΩ,[16] and a DC conductivity of about 200,000 S/cm.[32] The resistance of a metal-metal crossed-tube junction is approximately 500 kΩ,[14] with a DC conductivity of only 6,600 S/cm.[33] Consequently, the electrical conductivity of a CNT electrode can be improved by decreasing the junction resistance, increasing the tube lengths, or increasing the number of junctions. Other methods of improving the conductivity include improving the purity of the sample and doping the CNTs.

The easies method of improving the electrical conductivity of a CNT TCF is to increase the thickness and/or density of the electrode. Unfortunately, increasing the number of CNTs decreases the optical transmittance. Therefore a balance between the electrical and optical properties must be made. CNT electrodes are tunable to a specific sheet resistance or optical transmittance. Equation 3.1[7] provides an approximate relationship between the transmittance T and the sheet resistance R_s.

$$T = \left(1 + \frac{1}{2R_s}\sqrt{\frac{\mu_0}{\varepsilon_0}}\frac{\sigma_{op}}{\sigma_{dc}}\right)^{-2} \tag{3.1}$$

where σ_{op} and σ_{dc} are the optical conductivity and DC conductivity, and $\mu_0 \equiv 4\pi \times 10^{-7}\,\mathrm{Vs/Am}$ and $\varepsilon_0 \approx 8.854 \times 10^{-12}\,\mathrm{F/m}$ are the vacuum permeability and vacuum permittivity respectively. This relationship is valid for films thinner than a 380 nanometers with a much lower reflection than absorption, both true of CNT TCFs. The optoelectronic properties of a TCF are often described in a plot of transmittance verse sheet resistance, figure 3.3(a). The difficulty lies in decreasing the resistance without compromising optical performance. Figure

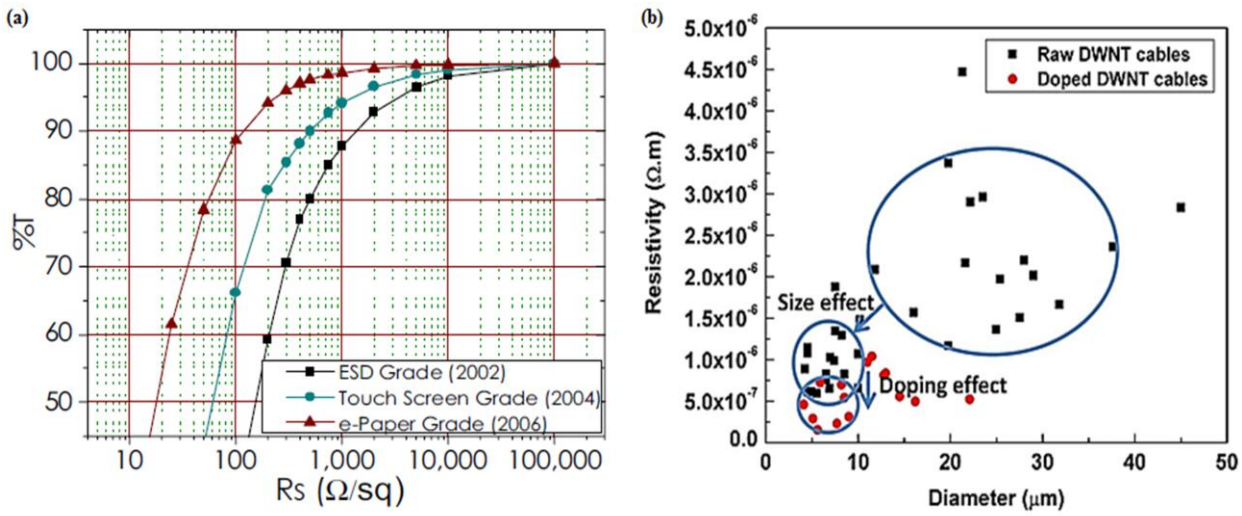

Figure 3.3. Percent transmittance verses sheet resistance for three different CNT electrodes.[34] (b) Resistivity improvements of CNT cables by debundling and doping.[35]

3.3(a) also shows that advances between 2002 and 2006 were able to decrease the sheet resistance by a factor of around 10 for most transmittance values.

Improvement of the electrical properties of CNT TCFs is usually done by decreasing the DC conductivity. Improving synthesis techniques to create long metallic SWNTs and DWNTs with minimal defects or impurities is one method of decreasing σ_{dc}. Other methods involve debundling the CNTs more effectively and improving the inter-tube electrical connections. A final method of improving σ_{dc} is to dope the CNT with n-type or p-type dopants. Figure 3.3(b) shows improvement in the electrical conductivity caused by debundling and doping. The goal of such modifications is to obtain an electrical conductivity 90,000 S/cm, equivalent to a 10 Ω/sq sheet resistance at 92% transmittance, which is the theoretical maximum.[7,36] Currently the best achieved DC conductivity is approximately 13,000 S/cm.[37]

3.2.2. Optical Properties. The transmittance of light through a CNT film is dependent on the optical absorption of CNTs (see section 2.2.2.) and the void fraction of the array. The void fraction is the ratio between the amount of free space and the area taken up by tubes at a given cross section of the film. Light passing through a film with a smaller void fraction is more likely to be absorbed. As discussed in the previous section, optical transmittance is a tunable parameter directly related to the sheet resistance because increasing the density and depth of the tubes increases absorption. The relation given by equation 3.1 is usually optimized by increasing the DC conductivity. Mathematically it stands to reason that decreasing the optical conductivity would be equally effective; however, the optical conductivity is difficult to change because it is directly related to the optical absorption and DOS of the CNTs. The optical conductivity is dependent on the tube structure, but this dependence is week and approximate value of 200 S/cm is used for all tube types.[7,38]

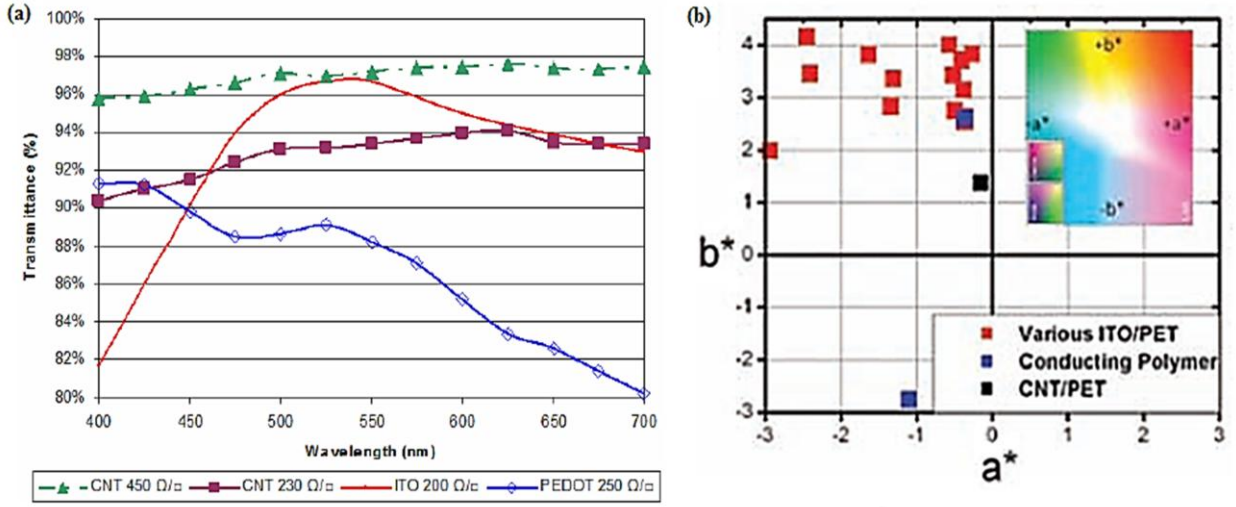

Figure 3.4. (a) Percent transmittance verses wavelength for a low resistance CNT, high resistance CNT, ITO, and PEDOT TCF.[34] (b) Color coordinates of a CNT film, ITO films, and conducting polymer films.[7]

The optical properties of CNT TCFs are often compared to other common TCF materials, including ITO and PEDOT (a conductive polymer). Parameters for comparison include the transmission spectrum, reflectivity, and color of the film. In these categories CNTs are very favorable. The refractive index of CNT electrodes is between 1.5 and 2,[7] which is slightly lower than that of ITO. This leads to less reflected light, or glare, which is beneficial for almost all applications. The transmission spectrum of CNT TCFs, see figure 3.4(a), is much smoother than that of ITO and PEDOT and it extends further into infrared and ultraviolet light. Transparency in these regions is advantageous for certain applications, including solar cells. The smoothness of the curve in the visible region makes CNTs more color neutral than ITO or PEDOT. Figure 3.4(b) shows the color coordinates for various TCF materials. CNTs are located close to the origin and therefor have a desirable gray color. Conversely, ITO films have an unwanted yellow or green tint and conductive polymers have a yellow or blue tint. It is important to note that CNTs films made from single chirality tubes will not be color neutral because of the limited energies of optical transitions permitted by a single DOS.

3.2.3. Mechanical Properties. In addition to an optical advantage over ITO, CNT films show vastly superior mechanical properties. In fact, the development of CNT TCFs will likely begin a new generation of flexible displays and touch panels. Like individual nanotubes, CNT TCFs have excellent strength and stiffness. CNT electrodes show no permanent resistance change for axial strains as high as 5%, whereas ITO electrodes exhibit permanent damage at ~2.5% strain and completely fail before 5% strain.[34] Figure 3.5(a) shows the percent change in resistance of a CNT TCF on a PET substrate for strains up to 18%. The PET substrate began plastic deformation at 5% strain at which point the resistance also showed irreversible change.[34] At 18% strain, the change in resistance was only 14%, which is less than in a plastically deforming metal.[34] CNT TCFs also outperform ITO TCFs in their ability to withstand cyclic

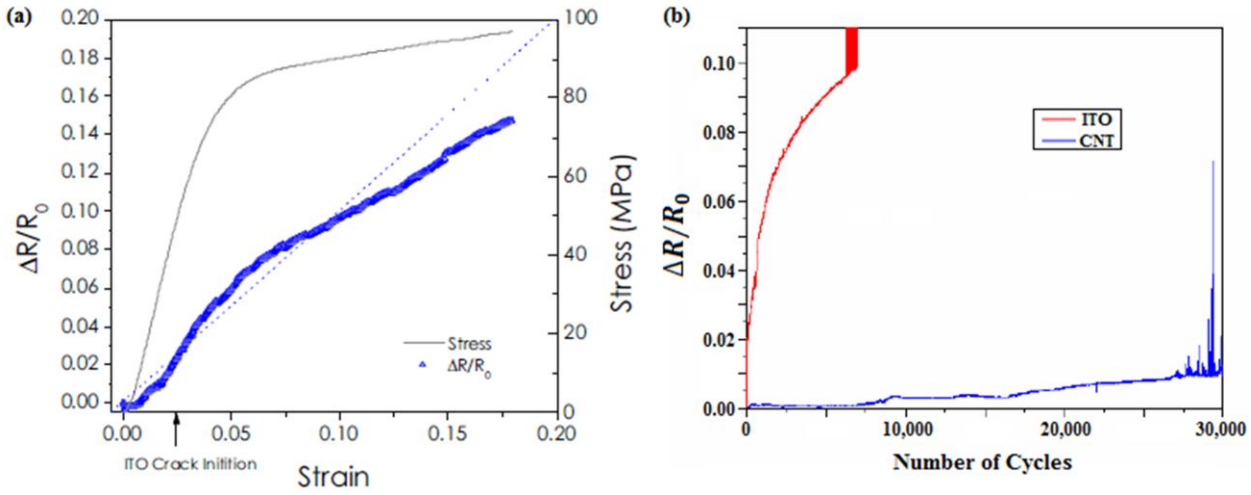

Figure 3.5. Percent change in resistance of a CNT electrode (a) loaded with uniaxial tension, (b) and exposed to cyclic loading.[34]

loading. CNTs have an extremely high Young's modulus and are largely unaffected by repetitive strains of 0.7%, shown in figure 3.5(b).[34] ITO on the other hand, degrades immediately at these values until failure at less than 7,500 cycles. In addition to mechanical robustness, CNTs are chemically inert and can withstand temperatures above 400°C.[30,31]

3.3. EXPERIMENT SAMPLES

3.3.1. Preparation. The CNT TCFs used in this experiment were created by spray coating glass with COOH functionalized MWNTs. The nanotubes were obtained in a suspension of deionized water from NanoLab Inc. NonoLab creates their tubes using CVD and functionalizes them through exposure to heated concentrated sulfuric and nitric acid.[26] The tubes are then washed and dispersed into deionized water using a probe ultrasonicator. The as purchased CNT suspension was mixed with ethanol to increase its volatility. Table 3.2 lists the properties of the CNT suspension used in these experiments. Using an airbrush, the solution was

Table 3.2. The properties of the CNT suspension that was used to make the TCFs studied in this report

Description	Value	Description	Value
Wall structure	MWNT	Outer Diameter	10-20 nm
Fabrication method	CVD	Length	1-5 μm
Purity	>95%	Solution type	Suspension
Chirality (conduction)	Mixed (conducting and semiconducting)	Solvent	50% DiH_2O/ 50% Ethanol by volume
Functional group	COOH	Concentration	0.5 g/L
Percent Functionalization	2-7 wt%	Stability lifetime	3-6 months

sprayed freehand onto a glass substrate. Heat treatment at 140°C was applied during the spraying, after it for 20 minutes, or not at all. The main difficulty in sample preparation was evenly spray-coating the glass substrate without allowing droplets to form. Heat treatment during the spraying was most effective because it prevented excessive wetting of the surface and lead to a more uniform film. Heat treatment also mildly annealed the samples thereby improving the electrical conductivity.

3.3.2. Properties. The properties of the pre-leaser annealed CNT TCFs were investigated using two and four point resistance measurements, optical and SEM imaging, and Raman spectroscopy (see section 5.1 for more information on the evaluation methods). Two point resistance measurements of 10×15 mm CNT electrodes were made in the long direction; the values typically ranged from 500 to 10,000 kΩ depending on the film thickness, density, and uniformity. The sheet resistance values for samples heated during the spray coating varied between 50 and 350 kΩ/sq. Optical observations by the naked eye and with 10x magnification were used to determine the sample uniformity; figure 3.6(a-b) shows a sample with acceptable uniformity, i.e. no coffee stain effects from wetting. SEM images were used to further investigate film uniformity and to determine the extent of bundling. Figure 3.6(c-d) shows a CNT TCF at 8,000 and 55,000 times magnification. These images show some impurities, the lighter specks in figure 3.6(c), and bundle diameters of nearly 100 nanometers. The Raman spectrum, figure 3.6(e), shows two peaks close to 1500 cm^{-1} that are believed to be the defect band (D-band) and graphite band (G-band). This indicates the high amount of defects created by the tube functionalization. The other peaks in the spectrum correspond to the glass substrate and light leakage from the surrounding.

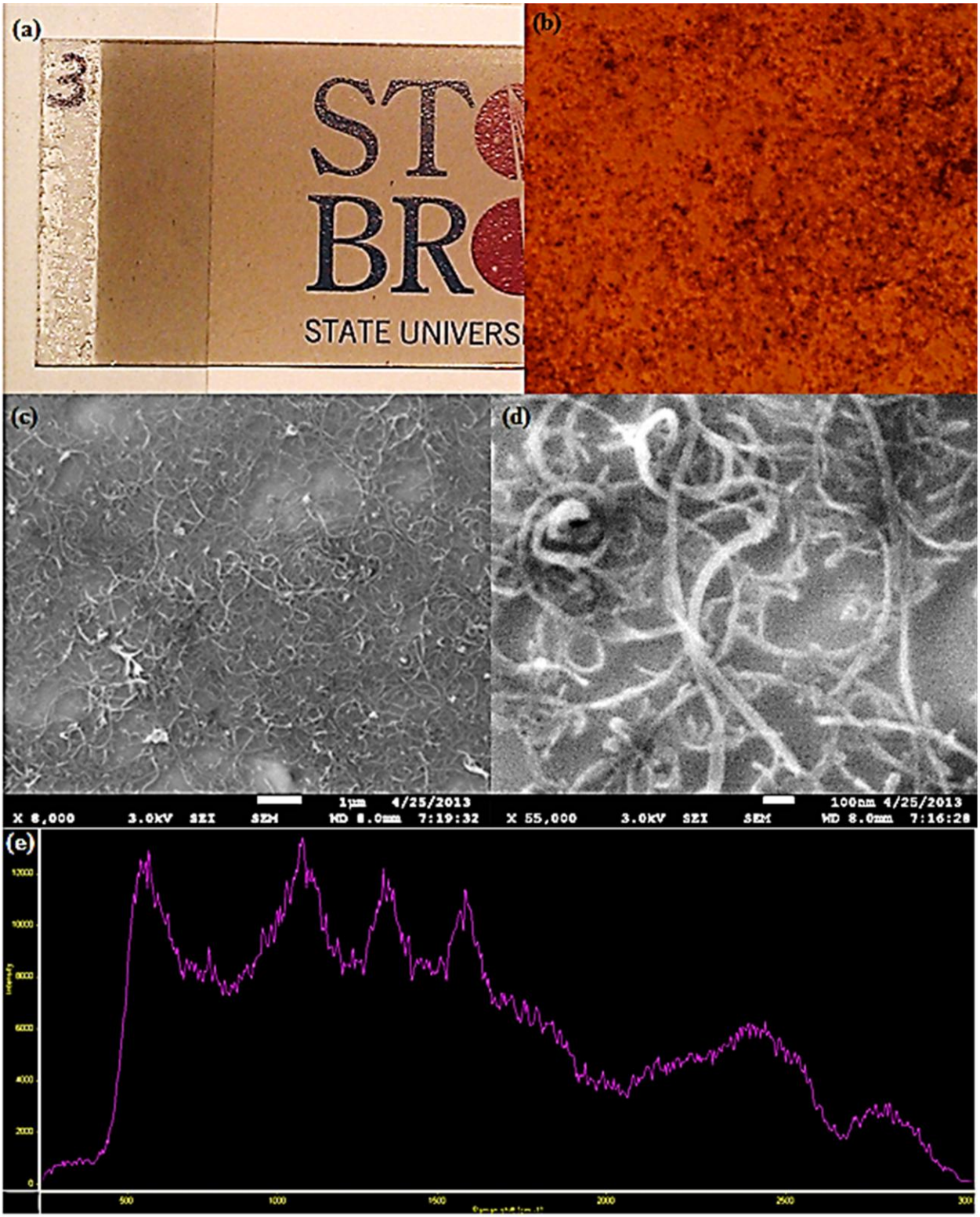

Figure 3.6. (a) Naked eye image of an as sprayed CNT TCF. (b) Optical image of a CNT TCF using 10x zoom. SEM images of a CNT TCF at (c) 8,000x and (d) 55,000x zoom. (e) The Raman spectrum for a CNT TCF.

4. LASER PROCESSING

The focus of this research is to use laser irradiation to thermally decompose the CNT's functionalization. LASER is an acronym for Light Amplification by Stimulated Emission of Radiation. Lasers emit beams of light that are spatially and temporally coherent. The strength of the beam varies from 1 mW laser pointers to 1000 W laser cutters. Laser annealing of CNT TCFs occurs at relatively low power (as low as 10 mW deepening on the setup) and laser removal of the CNTs occurs at approximately two orders of magnitude higher power. The properties of emitted laser light as well as laser heat transfer mechanism are important to understanding laser processing of CNT TCFs. Of particular interest are the laser defunctionalization, purification and removal of CNTs. The AERTC laser lab has a pulsed 532 nm and a pulsed 1064 nm laser that were used to process the CNT TCFs.

4.1. INTRODUCTION TO LASERS

4.1.1. Emitted Laser Irradiation. Lasers emit electromagnetic radiation that is spatially coherent and monochromatic; i.e. lasers emit light in a beam of only one color (wavelength). Characterization of the emitted light is important before laser processing can be discussed. The intensity profile of the laser beam is dependent on the physical makeup of the laser,[41] and is defined by a transverse electromagnetic (TEM_{nm}) modes. TEM_{nm} modes prevent electric or magnetic fields in the propagation direction.[42] Consequently, the *n* and *m* indices identify the number of horizontal and vertical nodes of high intensity respectively. TEM_{00} corresponds to a Gaussian beam profile which has only one node of peak intensity. A Gaussian profile exhibits the highest degree of symmetry and therefor will be discussed.

For a Gaussian beam profile, the intensity (I) at a specified point (r) and time (t) is expressed as,

$$I(r,t) = I_{pk}(t)e^{-\frac{2r^2}{\omega^2}} \tag{4.1}$$

where I_{pk} is the peak intensity and ω is the radius at which the intensity is less than the peak intensity by a factor of e^{-2}. Pulsed lasers transfer energy to a medium in an extremely short amount of time. A nanosecond laser delivers a pulse in one billionth of a second. This enables localized heating which is used to control surface processing.[43] For a pulsed laser, the energy of a single pulse (E_{pulse}) is given by,

$$E_{pulse} = \int_{-\infty}^{\infty}\int_{0}^{\infty} I(r,t)2\pi r\, dr dt \tag{4.2}$$

The pulse energy can be normalized by the area to provide the pulse fluence, $F = E_{pulse}/(\pi\omega^2)$. Nanosecond lasers are ideal for local annealing of the CNTs because the heat affected zone is only slightly larger than the beam diameter.[39] A continuous laser would lead to excessive

thermal penetration and potential damage of the substrate, and a femtosecond laser would provide no heat affected zone and would require excessive processing time.

In addition to the laser, it is important to consider the lens used to magnify the beam. The use of a lens decreases the beam's spot size and increases the beam's intensity. The two important parameters of a lens are the focal waist (ω_{02}) and the focal height (z_2). These represent the diameter of the beam at the focus point and the distance from the lens to the focus point respectively. For a Gaussian beam profile, their formulae are,

$$\omega_{02} = \frac{f\lambda}{\pi\omega_1} \tag{4.3}$$

$$z_2 = f + \frac{f^2}{2z_{R1}} \tag{4.4}$$

where f is the focal length of the lens, λ is the wavelength of light, ω_1 is the beam diameter at the lens, and z_{R1} is the Rayleigh length before the lens.

4.1.2. Laser Heat Transfer. Laser irradiation is able to heat a material by transferring the energy from the beams photons to the electrons and phonons of the material. When a laser beam strikes a material, the photons are either reflected, absorbed, or transmitted. The absorbed photons donate their energy to the electrons and atoms in the material. Photon-electron interactions are much more common than photon-phonon interactions because the electromagnetic properties of photons and electrons are more similar. The excited electrons interact with the atoms of the material. The resulting atomic vibrations, or phonon excitations, are observed as a change in temperature of the material.

In general, mathematical models for the absorption of energy rely on the assumption that the material is a continuum. Since a CNT TCF is not a continuum these models have limited use. As a first order approximation, the heat conduction from the laser can be expressed in terms of the temperature distribution (T) and the depth (z) using,

$$\rho C_p \frac{\partial T(x,y,z,t)}{\partial t} = \frac{\partial}{\partial z}\left(k\frac{\partial T(x,y,z,t)}{\partial z}\right) + \alpha Q(x,y,z,t) \tag{4.5}$$

where ρ is the density, C_p is the specific heat, α is the absorption coefficient, and k is the thermal conductivity of the CNT array, and Q is the laser power density.[1] This equation assumes that the CNTs are part of a continuum, one dimensional heat transfer, and that the absorbed energy is instantaneously converted into heat. The laser power density is defined as,

$$Q(x,y,z,t) = (1-R)I(x,y,t)e^{-\alpha z} \tag{4.6}$$

where R is the reflectivity of the CNT array. In addition to the assumptions of the equation, the values for the properties of the CNT array would have to be approximated. The resulting solution would contain significant error, and would not be able to describe the effect of laser irradiation

of a CNT array particularly well. Consequently, the work presented by this paper is based on qualitative and quantitative observations of the effect of laser irradiation of CNT TCFs.

There are two important parameters to the qualitative analysis of laser irradiated tubes. These are the number of pulses and laser exposure. These parameters are used to describe the amount of energy that the CNT TCF is being exposed to. The number of pulses is dependent on the scanning speed and beam size and is used to calculate the exposure. The exposure (e) is expressed in mJ/mm and is calculated by,

$$e = \frac{PN}{Af_{pulse}} \tag{4.7}$$

where P is the laser power, N is the number of pulses, A is the beam spot size, and f_{pulse} is the pulse frequency. The beam spot size is calculated from the focal waist as $A = \pi\omega_{02}^2$. The number of pulses is calculated by,

$$N = \frac{\omega_{02} f_{pulse}}{v} \tag{4.8}$$

where v is the scanning speed. The exposure is used to compare processing with different spot sizes, laser wavelengths, and number of pulses. Expressing the amount of laser irradiation in mJ/mm is used because it is normalizes the power by the affected area and number of pulses. The ideal processing exposure for different laser setups should match, but differences in peak intensity (equation 4.1) can lead to significant variation. Scanning with a larger spot size will lead to a less uniform exposure but will greatly increase the processing throughput. The exposure uniformity decreases because there is a greater difference between the average and peak exposures. And the processing throughput increases because the scan spacing and speed are simultaneously increased.

4.2. Laser Induced Thermal Defunctionalization

The primary focus of this research is to show improvement in the electrical conductivity of CNT TCFs made with functionalized tubes as a result of laser processing. Other research has already shown that conventional heating of functionalized CNTs at 900°C can remove the functional group and recover the conductive properties of pristine CNTs.[30] One major problem with this process is that even temperatures far below 900°C will damage glass and PET substrates. Laser heating is an alternative annealing method that can preferentially heat only the CNTs. This is possible because CNTs absorb light in the visible and IR ranges while transparent substrates do not. In addition, the use of a pulsed nanosecond laser limits the heat affected zone to an insignificant amount of the substrates surface. The CNT junctions are preferentially heated because the heat comes from multiple tubes. The CNTs are able to shed the functional groups without being damaged because thermal decomposition of molecules like COOH occurs at much lower temperatures than the damage threshold of CNTs. The laser annealing process follows several steps: (1) laser irradiation from a single pulse is absorbed by the CNTs, (2) the CNTs are

instantaneously heated by the photon-electron-phonon interactions, (3) the heated tubes shed their functional molecules and sp^2 carbon bonds are formed, (4) the sample cools and is hit with another pulse of photons. This time it takes for this cycle to occur is on the order on nanoseconds; if it took much longer, the CNTs would accumulate heat and the substrate could be damaged. Chapter 5 and 6 discuss the experimental procedures, evaluation methods, and results that support this thesis.

4.3. SECONDARY LASER MODIFICATIONS

4.3.1. Laser Purification. In addition to defunctionalizing the CNTs, laser irradiation is able to remove impurities from the film by laser ablation. Other work has shown that laser exposure at 6 mJ/mm^2 is able to purify non-functionalized CNTs by removing defective phases and amorphous carbon.[1] This provides additional improvement of the optoelectronic performance of laser processed CNT TCFs. The extent of purification is observed in the relative intensities of the D and G-bands of the Raman spectrum (see section 5.1.3). This effect is believed to be secondary for functionalized CNTs, and only accounts for a small amount of the improvement in the electrical conductivity. This is supported by the negligible purification seen in the Raman spectrum of processed CNT TCFs.

4.3.2. Laser Isolation. A third laser process that is useful in the development of CNT TCFs is laser removal of the CNTs. Removal of the CNTs was observed at laser exposures of less than 100 mJ/mm^2. The removal of CNTs causes the revival of the original transmittance of the substrate, and an open circuit in the electrode. Fortunately, CNTs were removed from the sample without damaging the glass substrate. In addition, the removed area is approximately the size of the laser spot size. A femtosecond laser may be able to create removal lines on the order of the CNT's diameters. Laser removal of the CNTs is particularly useful for creating patterned TCFs.

4.4. EXPERIMENT SETUP

The experiments presented in the following chapter use a 532 nm and a 1064 nm pulsed laser to scan small area CNT TCFs. Figure 4.1 shows the schematic representation and a picture of the laser setup. A Nd:YAG nanosecond laser from Yucco Optics is used. The laser beam passes through several optical components and is directed by mirrors before reaching the sample. A polarizer and partial beam splitter are used to control the power. A shutter is used to block the beam when not scanning, and a lens is used to decrease the beam spot size and increase the intensity. In addition, mirrors are used to direct the beam path through two apertures; the mirrors are adjusted to make sure the beam is normal to the sample.

The sample is placed on an Aerotech X-Y stage that moves in the plane perpendicular to the laser beam. The stage is controlled the computer program A3200 Motion Composer. A tilt stage is used to ensure the sample is normal to the beam. Also, the lens is attached to another motion stage that moves in the Z-direction (parallel to the beam) to control the focus. In-situ

imaging of the sample is acquired with a 1.3 MP Aptina Color CMOS digital camera. A filter is used to protect the camera from the laser beam. The samples are first scanned using high power to create an isolated rectangular area. Then they are raster scanned at the desired laser parameters. The primary focus of this work was on the effect of different power levels, but spot size and wavelength were also varied.

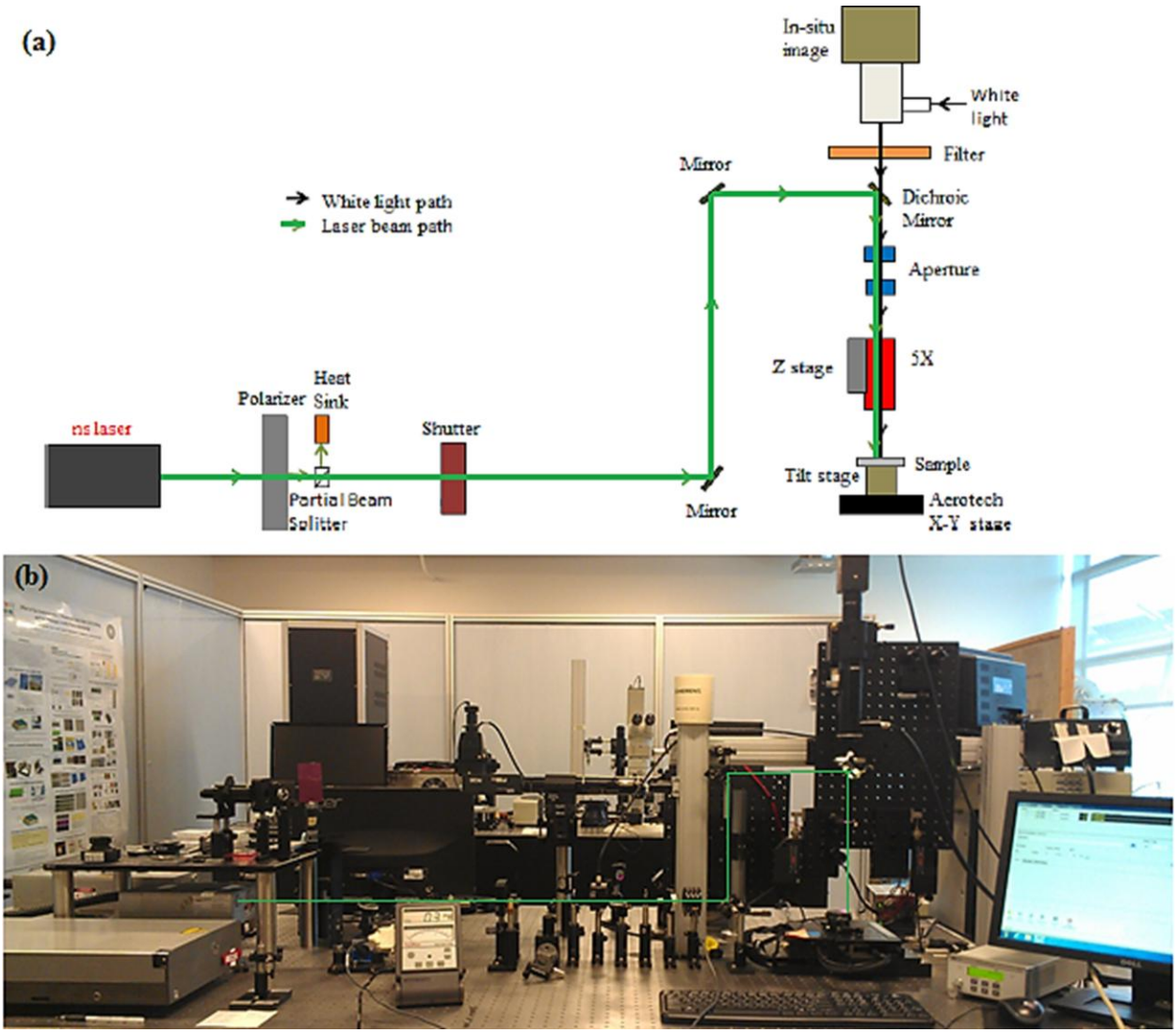

Figure 4.1. (a) Schematic representation,[25] (b) and picture of the laser setup.

5. EXPERIMENTAL RESULTS

Several experiments were implemented to study the characteristics of laser processed CNT TCFs. The primary focus is to show improvement and then deterioration of the electrical conductivity of CNT TCFs as exposure to laser irradiation increased. Additional experiments investigate the effects of conventional heating, the possibility of directional conductivity associated with laser scanning, and the stability of processed and unprocessed CNT electrodes. The outcomes of these experiments were observed with optical and SEM imaging, two and four-wire resistance measurements, and Raman spectroscopy. Note that this section is only a presentation of the results; their discussion is offered in chapter 6.

5.1. EVALUATION METHODS

5.1.1. Resistance and Sheet Resistance Measurements. Two and four-wire resistance measurements were used to evaluate the electrical conductivity of the CNT TCFs. The two-wire resistance values were used to obtain in-situ measurements that detect the relative improvement in conductance. The measurements were made by isolating an area, usually 10×15 mm, of a sample and attaching metal wires with silver paste to the opposing shorter ends; the setup is shown in figure 5.1(a). The lines used to isolate the rectangle extend to the edge of the sample to prevent electrical contact around the specified area. The resistance was then measured by connecting the wires to a digital multimeter. The two-wire resistance measurement is much quicker and easier to make and requires a smaller area than the four-wire sheet resistance measurement. The disadvantage is that the result is dependent on the geometry and wire resistance and cannot be used in a comparison with outside sources.

Four-wire sheet resistance measurements were made using Van der Pauw's method. Although the measurement process takes more time, the results are not dependent on the sample dimensions, and the resistance of the wires and contacts are automatically separated from the measurement. The four-wire setup, see figure 5.1(b), is similar to the two-wire setup; the difference is that a square area is used with the contacts in the corners. The contacts are labeled 1 to 4 counterclockwise starting with the top left. Van der Pauw's method involves supplying current to each pair of wires and measuring the resulting voltage across the opposite pair. In the notation used, V_{12} refers to the positive voltage between contacts 1 and 2. Similarly, I_{12} refers to the positive DC current flowing from 1 to 2. In total, eight resistance measurements are made; they are $R_{12,34}$, $R_{21,43}$, $R_{34,12}$, $R_{43,21}$, $R_{41,23}$, $R_{14,32}$, $R_{23,41}$, and $R_{32,14}$ where $R_{AB,CD} = V_{CD}/I_{AB}$. In a homogenous material these values should all be equal; however, the samples used in this study are inhomogeneous because of the poor control of spray coating. The vertical and horizontal resistances, R_v and R_h, are calculated using the following formulae,

$$R_v = \frac{R_{12,34} + R_{21,43} + R_{34,12} + R_{43,21}}{4} \tag{5.1}$$

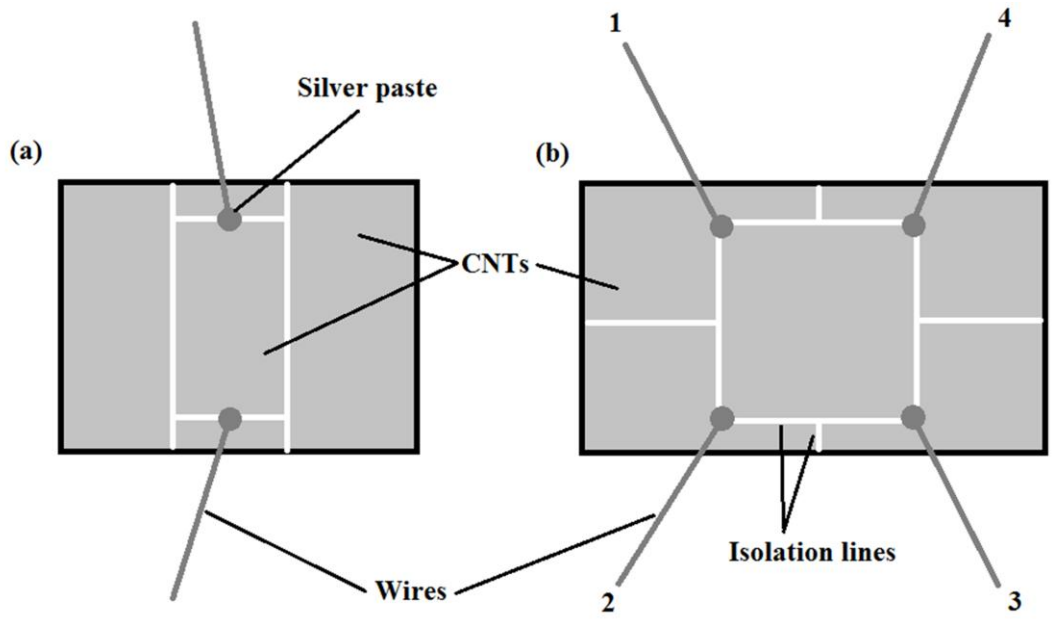

Figure 5.1. Schematics for (a) a two-wire resistance measurement, (b) and a Van der Pauw four-wire sheet resistance measurement.

$$R_h = \frac{R_{41,23} + R_{14,32} + R_{23,41} + R_{32,14}}{4} \tag{5.2}$$

And the sheet resistance is determined through the numerical solution of,

$$e^{-\pi R_v/R_s} + e^{-\pi R_h/R_s} = 1 \tag{5.1}$$

The sheet resistance values are particularly valuable because they can be compared with literature values for other CNT TCFs and with industry values of ITO TCFs. A HP 4156A Semiconductor Parameter Analyzer was used to supply the current and measure the voltage.

5.1.2. Optical and SEM Imaging. Optical imaging was performed with the naked eye, and under 10 and 20 times magnification. During the spray coating of the CNT TCFs, optical images were used to investigating the film quality. Images taken with no magnification were used to qualitatively determine the transparency, density/thickness, and uniformity of the CNT TCFs. Improved transmittance up to the complete removal of the CNTs could be detected for scanned samples. Optical microscopy at 10 and 20 times magnification provided more information about the film quality, including the extent of wetting during spraying. Optical microscopy was also able to detect damage done to the tubes. This was important in determining experiment parameters, in particular the scan spacing.

Scanning Electron Microscope (SEM) images were used for further magnification of the CNT TCFs. SEM images are captured by raster scanning the sample with a focused beam of electrons and collecting the resulting emissions. They describe the surface topology and composition of the sample and are used in combination with the electron beam's location to create the image. A Field Emission SEM with an in-line detector was used to characterize the

unscanned samples (see section 3.3). A Thermionic Emission SEM had to be used to image the scanned samples because the FE SEM was not available. Unlike the optical pictures, the SEM images show the individual bundles of nanotubes (figure 3.6). Additionally, they show CNT coated regions that are not detectable with the optical microscope. They provide information about the uniformity, bundling, and purity of the sample. Unfortunately, the images are not able to show the COOH functionalization of a single tube and thus cannot be used to determine the extent of defunctionalization.

5.1.3. Raman Spectroscopy. Raman spectroscopy was used in an attempt to identify the COOH functionalization and show its removal. The Raman spectrum is created by exposing the sample to low power laser irradiation and measuring the Stokes scattered light. The wavelengths of the Stokes shifted light correspond to vibrational modes of the sample. Since vibrational modes are specific to different atomic structures, the Raman spectrum can be used to identify the composition of the sample. The Raman spectrum of CNTs has several characteristic bands of peak intensity. These are the radial breathing mode (RBM) at ~200 cm^{-1}, the defect band (D-band) at ~1300 cm^{-1}, and the dual graphite band (G-band) at ~1600 cm^{-1}. The RBM mode can be used to solve for the average tube diameter by: $d_t = 227/\omega_{RBM}$.[40] The D-band provides information about the purity of the tubes; a low $I_D : I_G$ intensity ratio is desirable. And the G-band's dual G- and G+ peaks can be used to determine if the tubes are metallic, asymmetrical G-band, or semiconducting, suppressed G- peak.

To measure the spectrum of the CNT TCFs, a Raman spectrometer was created using a continuous green laser, a spectrum probe, and various lenses, mirrors, and filters. Figure 5.2 shows the schematic representation and a photo of the setup. The sample is exposed to laser irradiation from the green laser and the reflected and emitted light is directed toward the spectrum probe. This light is sent through a high band pass filter to eliminate the Raleigh scattered photons. Finally, the extremely weak Raman signal is focused through another filter and into the probe. The results from this setup agree with the manufacturer's information on the CNT solution; a D-band and a G-band are detected near 1500 cm^{-1}. Unfortunately, the signal does not have sufficient clarity to make out other features associated with the CNT TCF. Noise in the signal is the result of the Raman spectrum of the slide glass. One method of eliminating the noise is to use confocal Raman. Confocal Raman captures the signal from the region of the sample that is in focus and rejects everything else. In this way the CNTs can be characterized without the noise from the substrate.

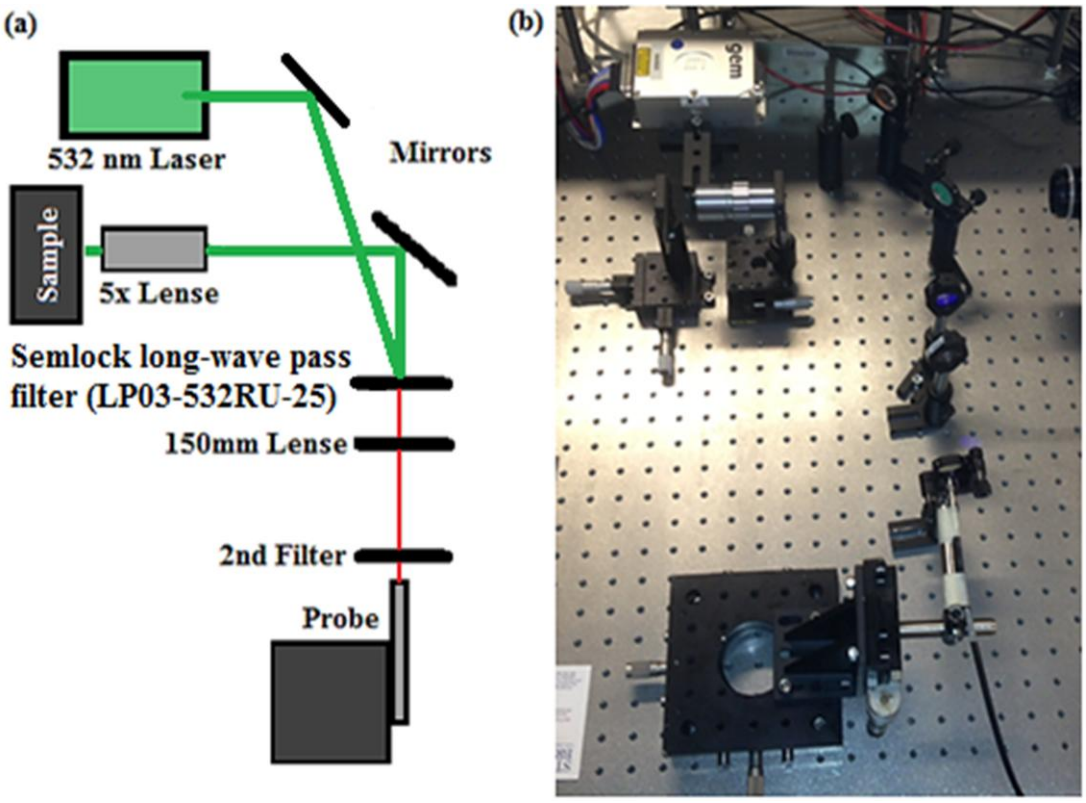

Figure 5.2. (a) Schematic representation, (b) and photo of the Raman spectroscopy setup.

5.2. EXPERIMENT DESCRIPTIONS AND RESULTS

5.2.1. Experiment A) Repetitive Laser Scanning. The purpose of this experiment is to measure the sheet resistance as a function of irradiative exposure for CNT TCFs. For each trial, a single 4-wire sample is prepared and its initial sheet resistance is measured (see section 5.1.1 for more information about sample setup and resistance measurements). The sample is scanned at an exposure level far below the optimal exposure, the point where the sheet resistance is minimized. The exposure amount is incrementally increased by varying the power and rescanning the sample. The sheet resistance is measured immediately after each scan. The power is steadily increased to provide multiple measurements before, near, and after the optimal exposure. The results are presented in a plot of the sheet resistance verses irradiative exposure.

Three trials of this experiment were performed using different laser wavelengths and magnification levels. The first trial used a pulsed 532 nm green laser and a 150 mm focal length lens. The second used the same laser a 5x magnifying lens. And the third trial used a pulsed 1064 nm laser and the 150 mm focal length lens. The three trials were performed on samples that were prepared in the same batch and had similar sheet resistances. Figure 5.3 shows the results of each trial and table 5.1 lists the full parameters of each trial. The exposure is calculated from these parameters using equation 4.7.

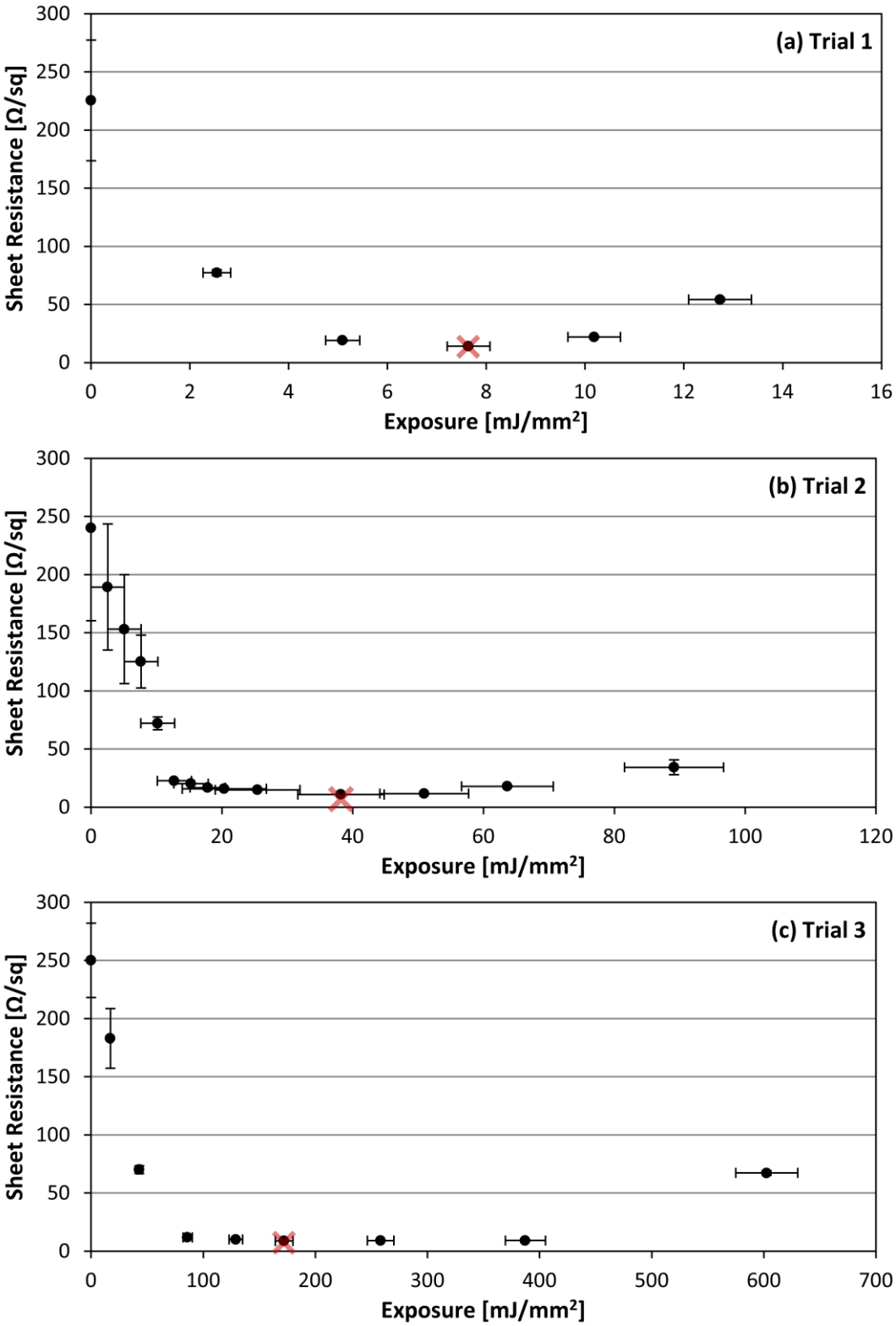

Figure 5.3. Sheet resistance verses exposure for CNT TCFs annealed with a (a) 532 nm pulsed laser with $\boldsymbol{D = 50}$ μm, (b) 532 nm pulsed laser with $\boldsymbol{D = 10}$ μm, (c) and 1064 nm pulsed laser with $\boldsymbol{D = 50}$ μm.

Table 5.1. The parameters for each trial of experiment A.

Parameter	Trial 1	Trial 2	Trial 3
Laser wavelength	532 nm	532 nm	1064 nm
Laser power	5-25 mW	0.2-7 mW	10-350 mW
Laser current	29.5 A	29.5 A	29.5 A
Laser frequency	10 kHz	10 kHz	10 kHz
Lens	150 mm	5x	150 mm
Spot diameter	50 µm	10 µm	8.6 µm
Focus height (above image focus)	14.5 mm	6 mm	2.5 mm
Scan speed	50 mm/s	10 mm/s	86 mm/s
Scan spacing	25 µm	5 µm	4.3 µm
Sample wiring	4-wire	4-wire	4-wire
Sample size	15×15 mm	15×15 mm	15×15 mm
Sample heating	During spraying	During spraying	During spraying

The error bars in figure 5.1 were calculated using the root-sum-square partial derivatives method. Their values should only be taken as approximate because several assumptions were made in their calculation. The error in the sheet resistance was approximated as,

$$\Delta R_s = \frac{\pi}{2\ln(2)}(\sigma_v + \sigma_h) \tag{5.1}$$

where σ_v is the vertical standard deviation (the standard deviation between $R_{12,34}$, $R_{21,43}$, $R_{34,12}$, and $R_{43,21}$) and σ_h is the horizontal standard deviation (the standard deviation between $R_{41,23}$, $R_{14,32}$, $R_{23,41}$, $and\ R_{32,14}$). This provides a good approximation for the error because homogeneous samples showed less variation in $R_{AB,CD}$ when measured multiple times. The error in the exposure, Δe, was calculated as,

$$\Delta e = \sqrt{\left(\frac{N\Delta P}{f_{pulse}A}\right)^2 + \left(\frac{P\Delta N}{f_{pulse}A}\right)^2 + \left(\frac{NP\Delta A}{f_{pulse}A^2}\right)^2} \tag{5.2}$$

where N is the number of pulses P is the laser power, f is the pulse frequency, and A is the beam spot size. To calculate the error in the exposure, the error in the number of pulses, and beam spot size had to be calculated;

$$\Delta N = \sqrt{\left(\frac{f\Delta D}{v}\right)^2 + \left(\frac{fD\Delta v}{v^2}\right)^2} \tag{5.3}$$

$$\Delta A = \frac{\pi}{2} D \Delta D \tag{5.4}$$

5.2.3. Experiment B) Individual Laser Scanning. This experiment is designed to further investigate the relationship between exposure and sheet resistance. In experiment A, there is some uncertainty associated with the effect of repetitive scanning. This experiment eliminates this effect by scanning the sample only once. Again, a single 4-wire sample is prepared and its initial sheet resistance is measured. This sample is scanned at the optimal exposure level determined from experiment A, and its sheet resistance is remeasured. Three samples with a similar resistance and from the same batch as those used in experiment A were chosen for this experiment. These were scanned under the conditions laid out in table 5.1, but only at the power corresponding to the optimal exposure. The results were plotted in figure 5.3 as red X's. In addition, table 5.2 lists the post-scanned resistance values used in the Van der Pauw method for each of the three samples. These trials are valuable because they give insight about the effect of repetitive scanning at the optimal exposure.

To investigate the effect of repetitive scanning across the entire range of exposures, several 2-wire samples were prepared. One of these samples was repetitively scanned as in experiment A. The others were each scanned once at a laser power below, near, or above the optimal exposure. All other parameters were kept constant. Figure 5.4 plots the two-wire resistances verses laser power for the repetitively scanned, and multiple single scan samples. Each point on the curve for the individual scan trial represents a different sample. The difficulty with this experiment is that the spraying process cannot provide very good uniformity between samples. As a result there is some error in the curve for the individually scanned samples.

Table 5.2. Resistances from the Van der Pauw method of measuring sheet resistance for three laser processed CNT TCFs.

Resistance	Trial 1	Trial 2	Trial 3
$R_{12,34}$	2.40	1.51	1.57
$R_{21,43}$	2.50	1.49	1.67
$R_{34,12}$	2.41	1.49	1.68
$R_{43,21}$	2.57	1.49	1.62
$R_{41,23}$	3.59	1.60	1.52
$R_{14,32}$	3.59	1.58	1.59
$R_{23,41}$	3.56	1.50	1.54
$R_{32,14}$	3.53	1.53	1.59
R_v	2.47	1.50	1.64
R_h	3.57	1.55	1.56
R_s	13.52	6.90	7.24

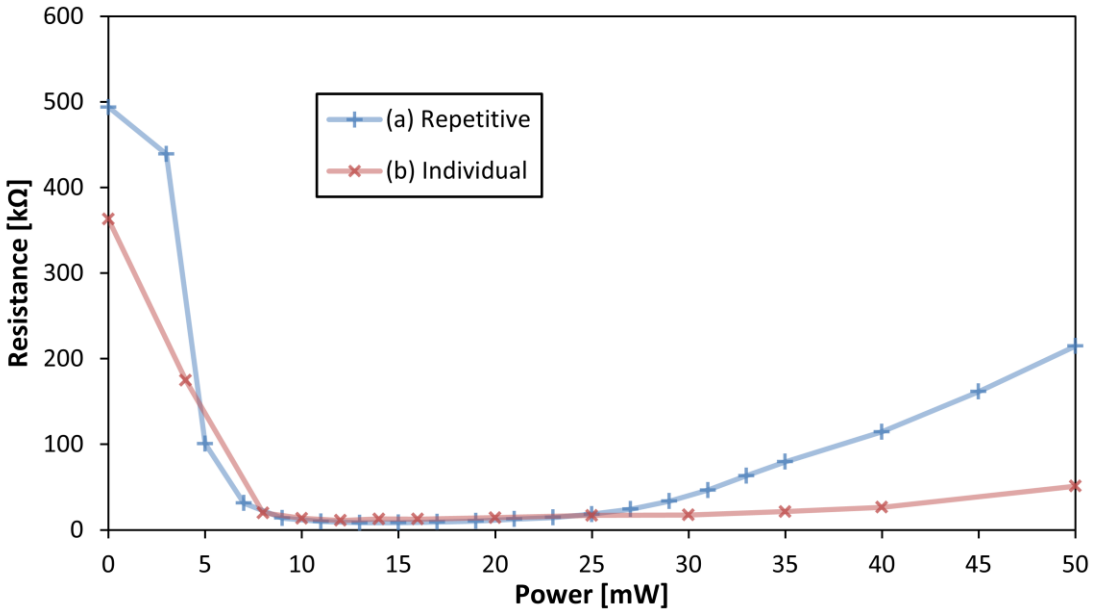

Figure 5.4. Two-wire resistance verses scan power for (a) a single CNT TCF repeatedly scanned at each power, (b) and for several CNT TCFs each scanned only once.

5.2.4. Experiment C) Low Temperature Thermal Annealing. The purpose of this experiment is to investigate the effects of thermal annealing. Other researchers have already shown that thermal annealing can improve the electrical conductance of a CNT TCF.[30] To measure the effect of conventional heating, a single sample was created and then separated into halves. One half was heated at 140°C for 20 minutes on a hot-plate, and the other remained unheated. After waiting a few days for the unheated sample to dry, the sheet resistance of each was measured. The unheated sample was determined to have a sheet resistance of 185 kΩ/sq, and the heated sample was determined to have a sheet resistance of 127 kΩ/sq.

In addition, the extent to which a conventionally annealed CNT TCF could be further improved using a laser was studied. To do this, a hot-plate heated sample and an unheated sample were repetitively scanned using the procedure from experiment A, and the laser parameters from trial 1 of table 5.1. To save time and effort, two-wire samples were used. A resistance verse power plot (figure 5.5) was created for a heated and an unheated sample with similar unscanned resistances.

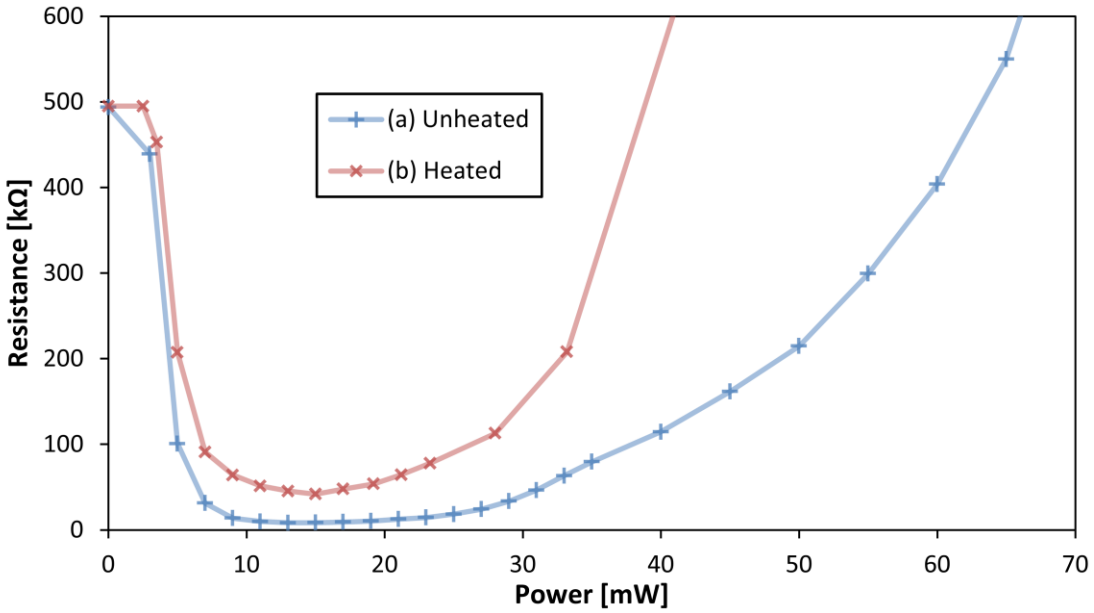

Figure 5.5. Two-wire resistance verses scan power for (a) an unheated CNT TCF (b) and a CNT TCF preheated for 20 min at 140°C.

5.2.5. Experiment D) Laser Induced Directional Conductivity. One characteristic of using laser heat transfer is that the exposure is not uniform. As a result, the electrical conductivity of the sample is extremely dependent on the scan spacing. This experiment is designed to investigate the effects of increasing the line spacing, and of scanning in both the horizontal and vertical directions. Three 4-wire samples are prepared and the initial horizontal and vertical resistances are measured using a multimeter. The samples are then scanned in the vertical direction with 20 mW, and the post-scanned horizontal and vertical resistances are measured. All parameters other than line spacing are kept the same. Sample 1 uses a line spacing of 25 microns, sample 2 uses 50 microns, and sample 3 uses 100 microns. The samples are then scanned in the horizontal direction with the same conditions, and the resistances are measured once again. The resistance measurements are listed in table 5.3.

Table 5.3. Horizontal and vertical resistance values for CNT TCFs scanned in the vertical and then horizontal direction. Each electrode was scanned at a different spacing, *S*.

Laser Process	Resistance	$S = 25$ µm	$S = 50$ µm	$S = 100$ µm
Unprocessed	R_v	1023	980	613
	R_h	602	854	346
20 mW vertical, 0 mW horizontal	R_v	30.14	125.6	191.3
	R_h	28.84	163.4	268.9
20 mW vertical, 20 mW horizontal	R_v	38.35	63.5	109.1
	R_h	31.88	54.9	86.3

5.2.6. Experiment E) Electrical Stability. This experiment was designed to determine the stability of laser annealed CNT TCF as time progresses. The two-wire resistances of an unscanned, optimally scanned, and damaged sample were measured for over a month (figure 5.6(a)). And the resistances of two optimally scanned samples were measured for 27 days (figure 5.6(b)). The samples were left out in the laboratory during the course of the experiment. The temperature of the room was set at 72°F and the humidity varied between 40 and 60%. Linear regressions were fit to each dataset; the slope of the lines indicates the change in resistance that occurs in one day. In figure 5.6(a), the slopes of the unprocessed, optimized, and damaged datasets are -13.3, 0.9, and 12.7 kΩ/day respectively. In figure 5.6(b), the slope of the 12 mW scanned sample is 0.14 kΩ/day and the slope of the 14 mW scanned sample is 0.19 kΩ/day.

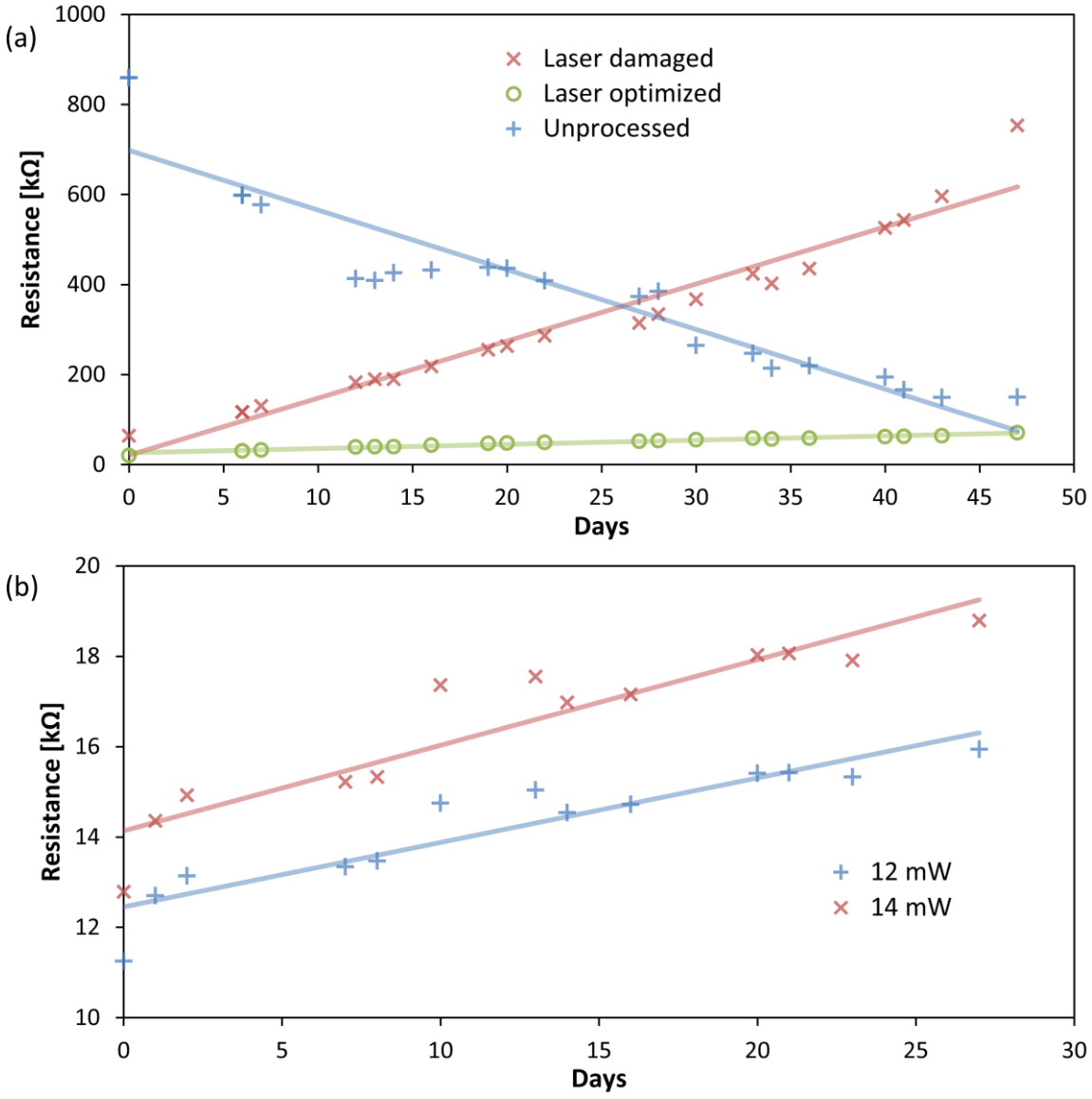

Figure 5.6. The change in resistance over time for (a) a damaged, optimized, and unscanned CNT TCF, (b) and two better optimized CNT TCFs.

5.2.7. Experiment F) Optical, SEM, and Raman Imaging. As discussed in sections 5.1.2 ad 5.1.3, optical, SEM, and Raman imaging were used to qualitatively evaluate the purity, uniformity, transmittance, composition, and bundle diameter of the CNT TCFs. In addition, each of these imaging techniques is able to show the effect of laser processing. Three samples were prepared and their right halves were scanned at the optimal exposure. Each sample was then characterized using optical, SEM, and Raman microscopy. The zero-magnification optical images (figure 5.7) show improved transmittance for the scanned side (right side) of each sample. The optical microscope images (Figure 5.8) clearly show the scan lines, and apparent removal of the CNTs. This is verified by the Raman spectrum (figure 5.9) which shows a significant reduction in the intensities of the D and G-bands. However, the SEM images (Figure 5.10) show the existence of CNTs within the scan lines.

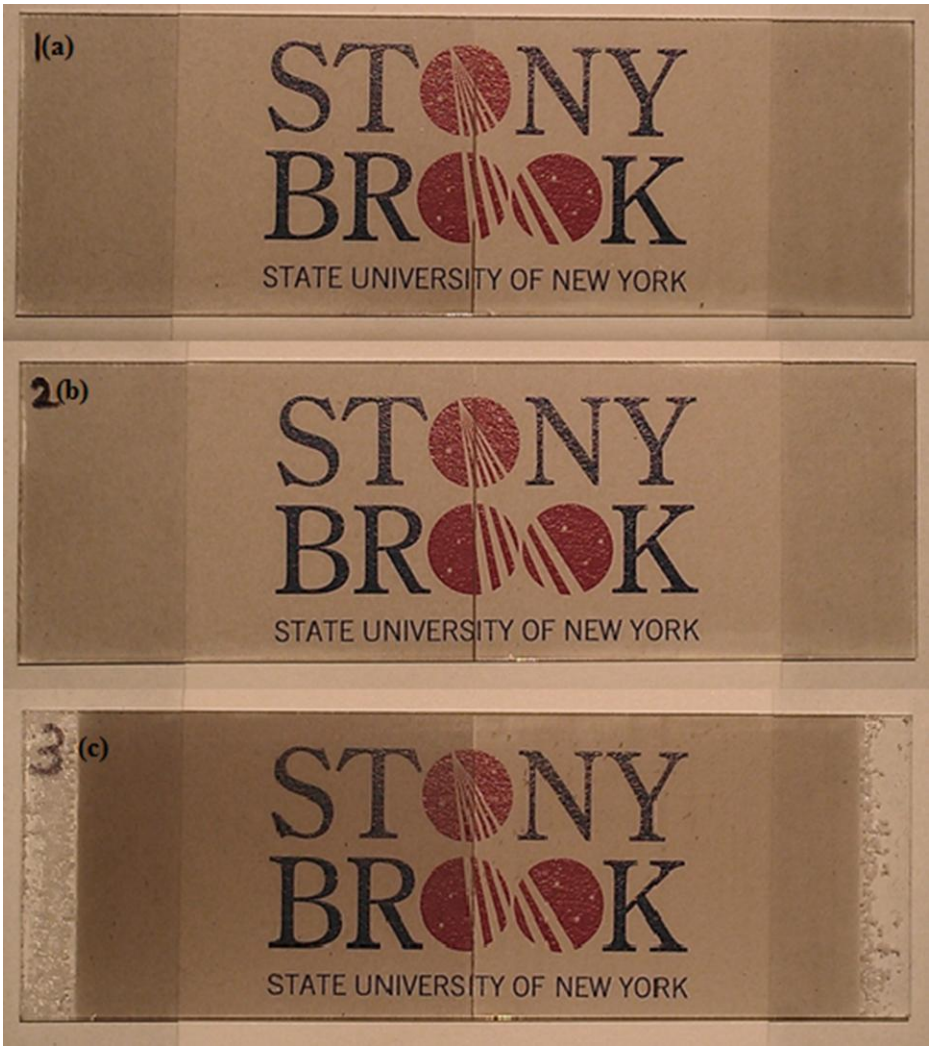

Figure 5.7. Naked eye optical images of CNT TCFs that were (a) not heated, (b) heated at 140°C for 20 min after tube deposition, (c) and heated at 140°C during spray coating. The left and right side of each TCF are unscanned and scanned respectively.

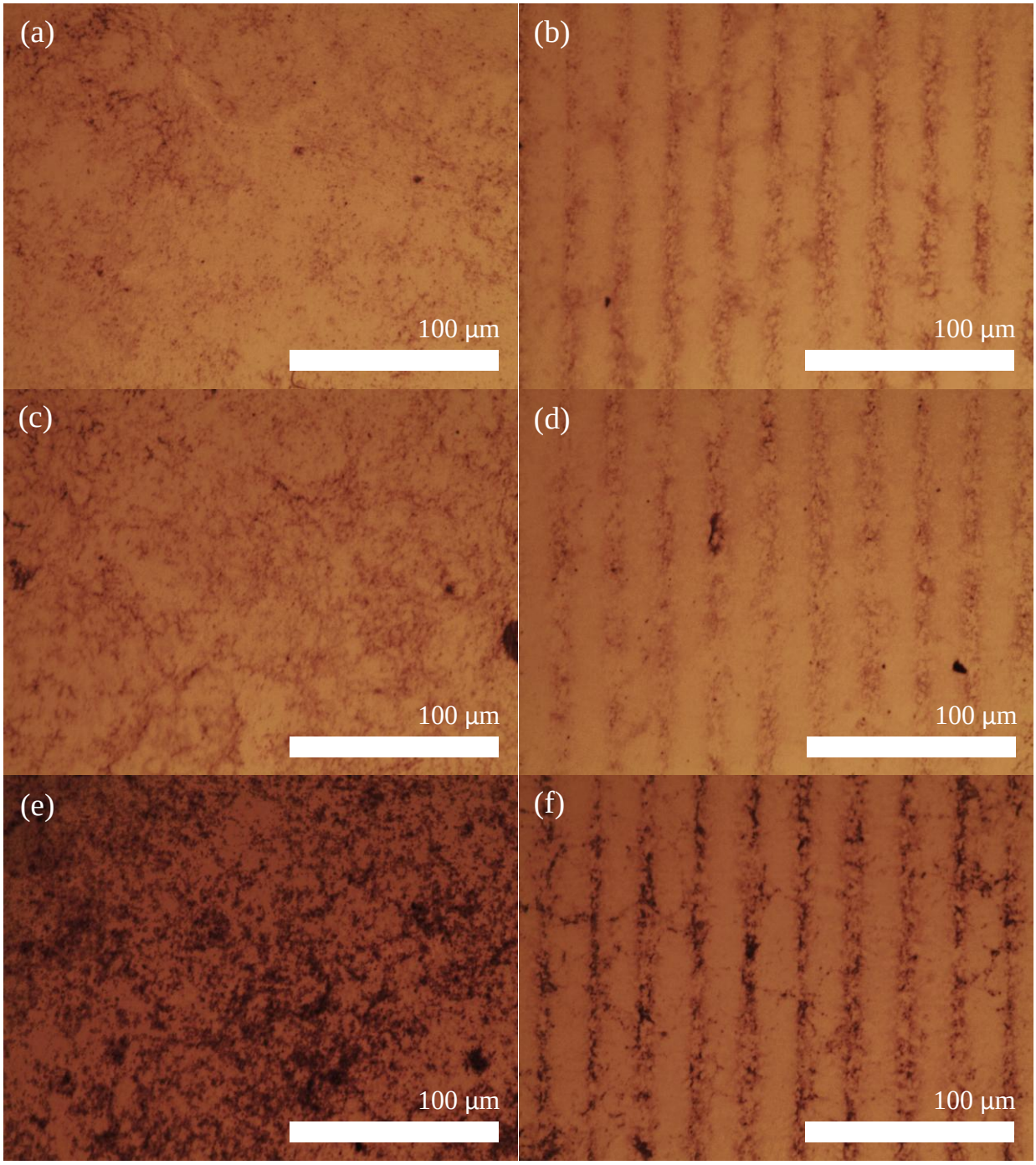

Figure 5.8. 20x magnified optical images of CNT TCFs that were (a) not heated, (b) heated at 140°C for 20 min after tube deposition, (c) and heated at 140°C during spray coating. The left and right side of each TCF are unscanned and scanned respectively.

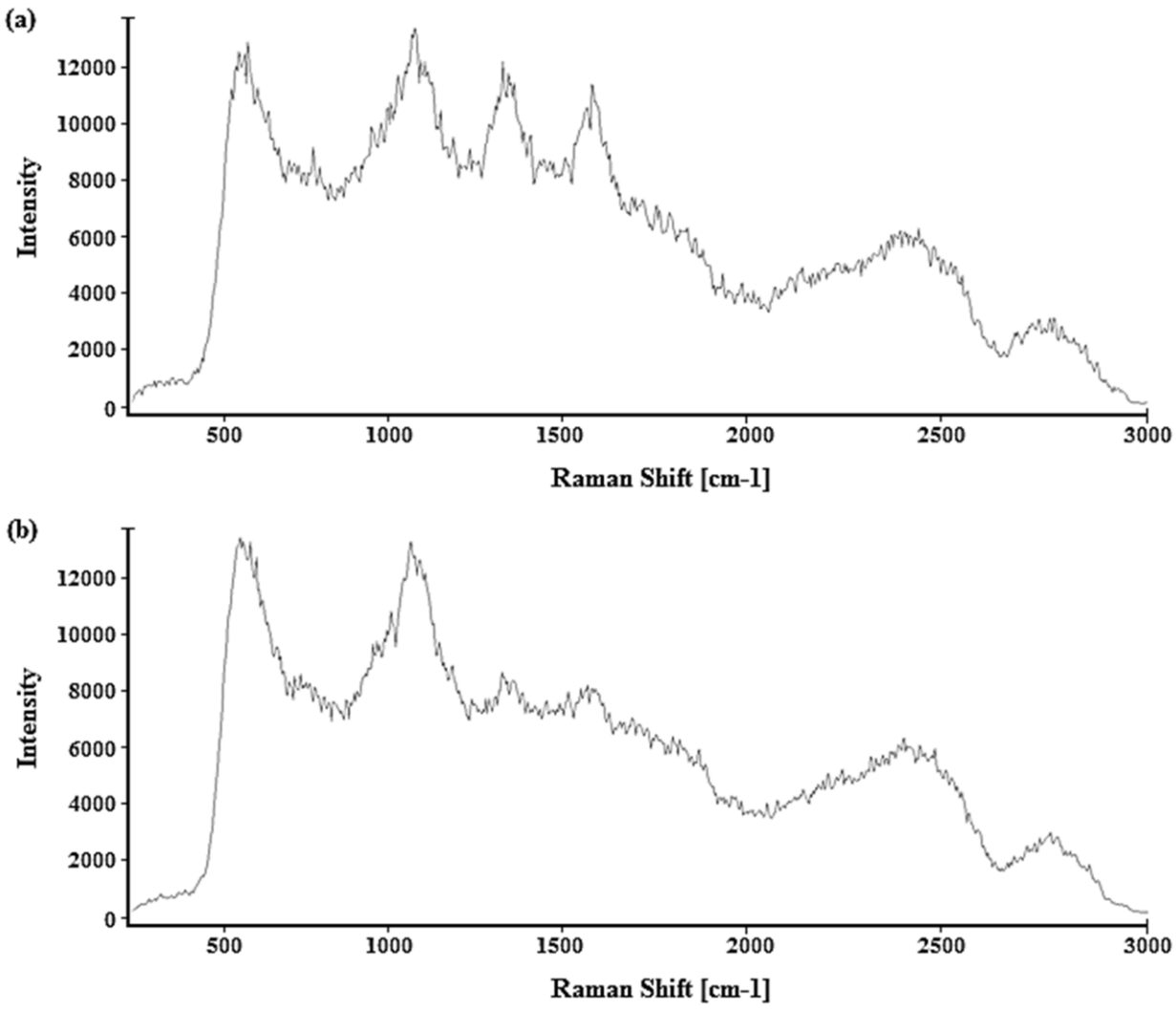

Figure 5.9. The Raman spectrums for a CNT TCF (a) before and (b) after laser scanning. Most of the spectrum is unrelated to the CNTs themselves.

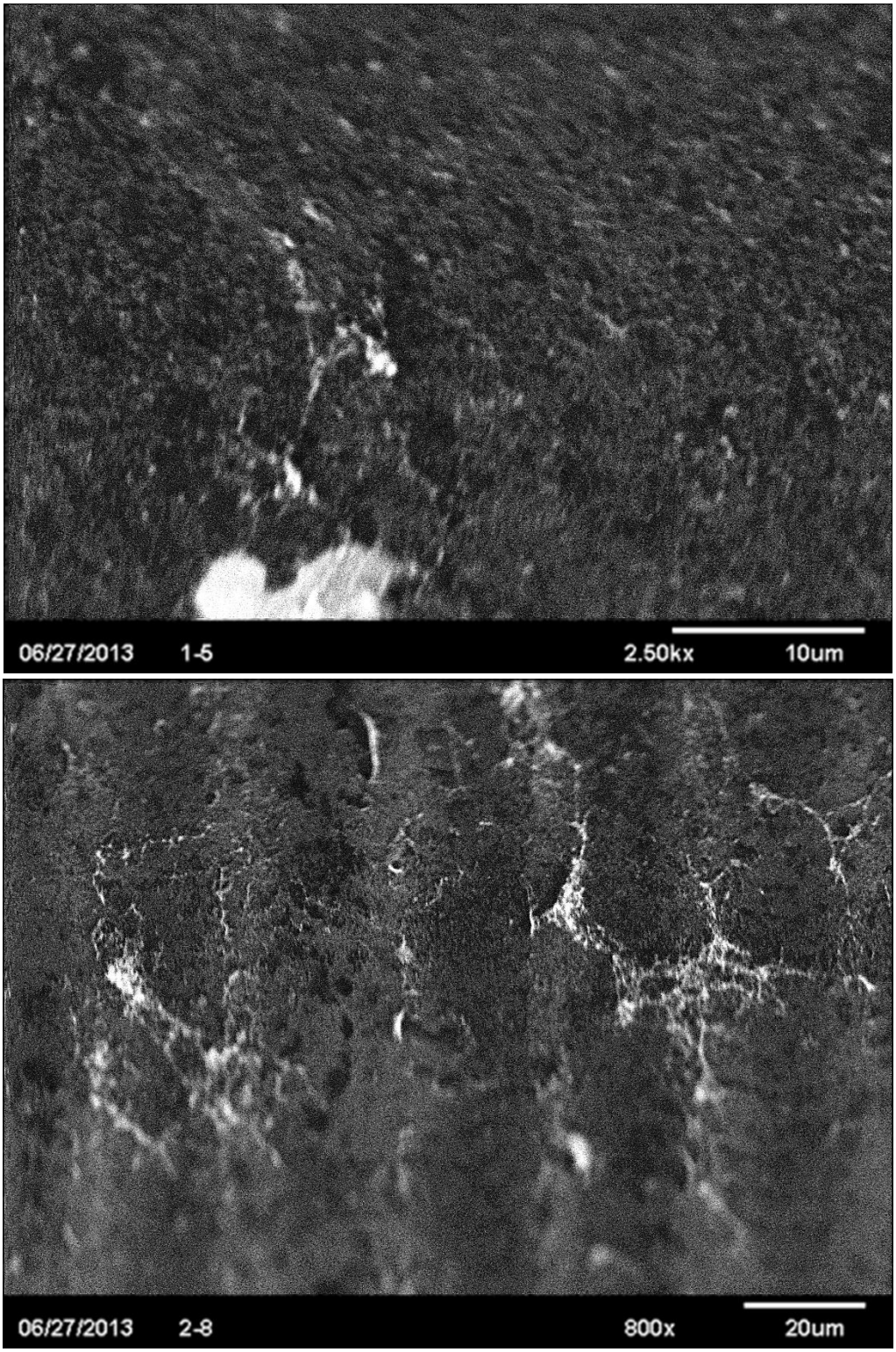

Figure 5.10. SEM images of a CNT TCF (a) before and (b) after laser scanning.

6. POST PROCESSED ELECTRODE PROPERTIES

This research asserts the claim that laser annealing is capable of improving the properties of CNT TCFs. Chapter 5 describes the experiments used to characterize these films, and lists the most relevant data that was obtained. These results confirm that laser annealing is able to vastly improve the optoelectronic performance of CNT TCFs. The main effect of laser irradiation is observed in the improvement of the electrical conductivity. In addition, at sufficient exposures, the transmittance of the CNT TCFs improves as material is removed. The stability of the electrodes was also addressed, although more work is required to make the CNT TCFs mechanically robust.

6.1. ELECTRICAL CONDUCTIVITY

The sheet resistances of three similar CNT TCFs were reduced by 92 to 97% by exposure to a single dose of laser irradiation. Figure 5.3 shows the dramatic effect of irradiative exposure at different frequencies and magnifications. Exposure to 532 and 1064 nm wavelength laser beams were both able to improve conduction by a factor of more than 34. While the optimal sheet resistances were similar, the 1064 nm laser beam required significantly more power to anneal to this level. This indicates that either the CNTs preferentially absorb green light, or higher energy photons are more effective at inducing the required structural changes. The second method is far more likely because CNTs absorb a similar amount of light in the visible and IR ranges,[31] but are more effective at absorbing light as higher energy (see section 2.2.2.)

At higher a magnification level, the laser beam required more energy to anneal to the optimal point but was more effective at reducing the resistance. Both effects are most likely caused by the difference in spot size. Since the beam profile is Gaussian and exposure is calculated per unit area, a larger spot size corresponds to a higher peak intensity. As a result, scanning with a higher magnification lens will minimize optimal exposure point. However, the electrode will not show the same degree of improvement because the film will be less uniform. The difference in the film uniformity can be seen in the variation of the resistance measurements made to calculate the sheet resistance (Table 5.2.). The standard deviation between the eight values of $R_{AB,CD}$ is an order of magnitude higher for a large spot size (trial 1) than for a small spot size (trial 2 and 3). Film uniformity can be improved at any magnification by optimizing the scan spacing. However, this can be difficult because the optimal exposure is dependent of the scan spacing.

The optimal resistance determined from repetitive scanning strongly agrees with the sheet resistance from a single scan at the same exposure, implying that the affect repetitive scanning is negligible up to the point of minimal resistance. This supports the conclusion that no appreciable damage is done to the CNT film by low power scanning and that a single scan at the optimal exposure can capture all the benefit of laser treatment. This also verifies that the laser setup was able to rescan along the same lines. At higher levels of exposure, repetitive scanning facilitates

quicker degradation of the electrical properties of the CNT film (Figure 5.4.). This shows that damage to the CNTs does accumulate. While significant for determining the minimum exposure necessary for complete removal of the CNTs, this does not affect the optimal exposure level.

It is important to show that laser annealing can more effectively improve the optoelectronic properties of CNT TCFs than conventional heating, e.g. with a hot-plate. Figure 5.5 shows the relative improvement of the resistances for a conventionally heated and an unheated CNT TCF exposed to laser irradiation. The results show a dramatic improvement in both cases; however, the preheated CNT TCF was not able to achieve as low of an optimal resistance as the unheated one. This is attributed to structural difference between the CNT arrays, because both electrodes would not have had the same unannealed resistance. For similar CNT TCFs, a conventionally annealed film will show a 30% improvement of the sheet resistance. Further improvement may be possible at higher temperatures, but heat treatment at temperatures appreciably above 140°C can potentially damage the substrate, particularly if PET is used.

Laser heat transfer is able to heat the CNTs to extremely high temperatures without damaging the substrate because the thermally enhanced region is much smaller than the substrate thickness. Consequently, CNTs can also be selectively removed, thereby creating an open circuit and regenerating the original uncoated substrate transmittance. Removal of the CNTs could be the result of vaporization but it is more likely that the CNTs are simply stripped from the substrate. Laser removal of the CNTs can be used to pattern the electrode which is useful in numerous applications, including touch panels. Laser heat transfer can also be used to selectively anneal CNT TCFs. Table 5.3 shows that an electrode with preferred directionality can be created by increasing the scan spacing so that unscanned material exists between scan lines. An electrode with a 40% higher resistance in the direction perpendicular to the scan lines was created. Higher directionality could be created by increasing the scan spacing but a diminishing return exists because increasing the spacing decreases resistance in both directions. Experiments also showed that the directionality can be destroyed by scanning the CNT TCF in the other direction.

6.2. OPTICAL TRANSMITTANCE

In addition to improved electrical conductivity, CNT TCFs scanned at the optimal exposure show improved optical transmittance (figure 5.7.). The 20x magnified optical images and Raman spectrum show that transmittance is improved through partial removal of the CNT film. The optical microscope images show significantly improved transparency within the center of each scan line and little effect elsewhere. These optically enhanced lines are less than half the size of the scan lines. This indicates that there is a threshold exposure level beyond which the film is significantly altered. The apparent removal of the CNTs is contradicted by the improved electrical conductivity perpendicular to the scan lines (see section 5.2.5). In addition, the SEM images show that the film composition at the center of the scan lines is similar to unscanned film. Therefore the apparent removal of CNTs seen in the optical images is actually only partial removal of the film and is possibly associated with purification. The improved transmittance is

likely caused by the removal of amorphous carbon and excess functional molecules that were deposited with the CNTs.

The transmittance can be increased further by scanning the film with exposure levels higher than the optimal exposure. At very high power levels, the CNT film is completely removed, the original transmittance of the substrate is restored, and the conductance of the electrode is fully diminished. By scanning at different exposure levels, the optoelectronic characteristics of a CNT TCF can be tuned. This is similar to the optoelectronic tuning achieved by increasing the sample thickness (see section 3.2.1.). It would be interesting to see if quantitative measurements of the transmittance and sheet resistance provided a point with better performance than the minimal sheet resistance. A CNT TCF could be made with worse transmittance than ultimately desired and laser irradiation could be used to obtain the final optoelectronic properties. CNT TCFs prepared this way may be more completely annealed and thereby show better conductance at a given transmittance.

6.3. ELECTRODE STABILITY

The electrode stability is an important parameter for determining if the improvement observed by laser irradiation will be feasible in production quality CNT TCF. Many of the doping methods that achieve some of the lowest sheet resistances for CNT TCFs are not stable at room temperature and therefore are impractical as of yet. Figure 5.6(a) shows the change in resistance over time for a scanned, unscanned, and damaged CNT TCF. The damaged and unscanned CNT electrodes exhibit poor stability over time. The unscanned electrode's resistance decreased at a rate of approximately 13 kΩ/day. Initially, it was believed that the decreasing resistance corresponded to the drying of the sample; however, after over a month of steady decline, it seems that the CNTs must be undergoing a structural change. On the other hand, the resistance for the damaged CNT TCF steadily increased at a rate of 13 kΩ/day. It is believed that unstable electrical connections were made by the laser scanning process and that these connections are degrading over time. Fortunately, laser processing near the optimal exposure seems to do a good job of stabilizing the electrode (figure 5.6(b)).

For CNT TCFs processed to the minimum resistance, the change in resistance over time is less than 0.2 kΩ/day. This electrical stability is attributed to regenerated sp^2 carbon bonds,[30] and improved inter-carbon electrical connections. In addition, mechanical stability of the film may have been enhanced by improved adhesion to the substrate. Softening of the surface of the glass may have led to slight immersion of the CNTs. In figure 5.6, the similarity in the day-to-day changes of the CNT electrodes indicate that the ambient conditions, most likely humidity, have an effect on the electrical conductivity. The mild change in resistance associated with the conductive CNT TCFs is acceptable for these preliminary studies. A commercial quality CNT TCF would have an additional coating to protect the CNTs and that would presumably improve stability.

7. FURTHER WORK

The dramatic improvement in the electrical conductivity shown in the previous chapters establishes laser processing as a viable method of creating CNT TCFs. However, more work needs to be done before CNTs replace ITO as the prevalent TCF. In addition, further theoretical and experimental analyses could provide more information about laser annealing.

7.1. Obtaining a Clearer Picture. Future work on the development of the laser annealing process should include a more accurate model for the temperature profile resulting from laser exposure. As mentioned in section 4.1.2, the current model does not account for the CNT film not being a continuum. A better model could be used to determine the temperatures associated with the laser annealing and removal processes; this would be valuable in a comparison with conventional annealing. Also, the model could be used to predict the effect of different laser parameters and provide theoretically optimized values.

In addition, further evaluation of the optoelectronic properties should be performed. In particular, a transmittance verses resistance curve should be made by changing the exposure level. Such a curve will be useful in tuning a CNT TCF's properties and might provide a clear optimal exposure level for both transmittance and electrical conductivity. Additional imaging of the sample should also be performed to investigate the extent to which the functional group is removed. Possible methods include TEM images similar to those shown in figure 3.2, and Confocal Raman as mentioned in section 5.1.3. Clear evidence of the removal of the functional group would support the claim that annealing improves conductivity by defunctionalizing the CNTs. In addition, better SEM images should be obtained to support those presented in this report (see section 5.2.7).

7.2. Development of CNT TCFs. In addition to further work with the annealing process, steps should be taken to develop a functional, high quality CNT TCF. Important steps include obtaining samples with a high initial electrical conductivity and attempting further improvement by laser annealing. The CNT TCF prepared for this research showed an initial sheet resistance of on the order of 100 kΩ/sq and were improved by more than 20 times. CNT TCFs from literature have resistances as low as 100 Ω/sq; an order of magnitude improvement of these would make CNTs an extremely strong competitor in the TCF market.

Additionally, laser processed CNT TCFs should be made more robust and the mechanical and electromechanical properties should be evaluated. CNT TCFs have the potential for extremely good mechanical performance (see section 3.2.3). Laser annealing could possible improve this performance further. Also, a flexible CNT TCF should be created to show potential new applications available through the use of CNTs.

8. CONCLUSION

The demand for TCFs has increased with the popularity of touch screens, LCDs, OLEDs, and solar cells. Currently ITO is used for most of these applications, but the next generation of TCFs will most likely be made using nanomaterials. CNT TCFs have the potential to be cheaper, more manufacturable, and better performing than ITO TCFs. The main obstacle to overcome before high quality CNT TCFs can be realized is their poor electrical conductivity. Conventional thermal annealing has been proven as one method of improving the electrical conductivity of functionalized CNT TCFs. This research presents an advanced annealing method using laser irradiation.

Pulsed laser heat transfer is used to preferentially heat only the CNTs and limit the heat affected zone to the CNT film thickness. Heated CNTs cause thermal decomposition of their functional groups without damaging the tubes or the substrate. In this manner, the sheet resistances of three similar CNT TCFs were reduced by 92 to 97%. This level of improvement is far superior to the improvement observed by conventional thermal annealing. Laser beams of 532 nm and 1064 nm light were both able to improve the electrical conductivity by a factor of approximately 25. The CNT TCFs were best optimized using high energy photons and a small scan spacing. The optimal exposure, the exposure at which the resistance is minimized, depends on the laser parameters but is generally low.

Repetitive scanning was presented as an accurate method of determining the optimal laser power for single scan processing. In addition, a new method of tuning the optoelectronic performance is offered. Scanning at above the optimal exposure improves transmittance while electrical conductivity degrades. Thermal annealing was shown to improve electrode stability; scanning at the optimal exposure decreased the degeneration of the electrode from 13 kΩ/day to 0.2 kΩ/day. Also, selective laser annealing was presented as a method of creating directional resistance panels without having to pattern; 40% directionality was achieved with no optimization. Patterning was performed by laser removal of the CNTs and was able to create isolated conductive paths in the electrode.

Further work should be done to develop a mathematical model of the heating of the tubes. This could be used to understand and optimize annealing. Also, additional measurement should be made to further the results that are presented here. Finally, a high performance CNT TCF should be developed by laser annealing a sample made with higher quality tubes and a better deposition method.

REFERENCES

[1] T. Ueda, S. K. (2008). Effect of laser irradiation on carbon nanotube films for NOx gas sensor. *Surface & Coatings Technology, 202*, 5325–5328.

[2] *Corning® Boro-Aluminosilicate Glass Products*. (n.d.). Retrieved July 28, 2013, from DELTA Technologies, LTD: http://www.delta-technologies.com/products.asp?C=1

[3] Xueshen Wang, Q. L. (2009). Fabrication of Ultralong and Electrically Uniform Single-Walled Carbon Nanotubes on Clean Substrates. *Nano Letters, 9*(9), 3137–3141.

[4] T. Dürkop, S. A. (2004). Extraordinary Mobility in Semiconducting Carbon Nanotubes. *Nano Letters, 4*(1), 35-39.

[5] Zhen Yao, C. L. (2000). High-Field Electrical Transport in Single-Wall Carbon Nanotubes. *Physical Review Letters, 84*(13), 2941–2944.

[6] Min-Feng Yu, O. L. (2000). Strength and Breaking Mechanism of Multiwalled Carbon Nanotubes Under Tensile Load. *SCIENCE, 287*, 637-640.

[7] David S. Hecht, L. H. (2011). Emerging Transparent Electrodes Based on Thin Films of Carbon Nanotubes, Graphene, and Metallic Nanostructures. *Advanced Materials*(23), 1482–1513.

[8] Monthioux, M. (2006). Who should be given the credit for the discovery of carbon nanotubes? *CARBON, 44*(9), 1621-1623.

[9] *File:CNTnames.png*. (2006, October 1). Retrieved July 28, 2013, from Wikipedia: http://en.wikipedia.org/wiki/File:CNTnames.png

[10] *carbon nanotube chirality / lászló péter biró*. (n.d.). Retrieved July 28, 2013, from visualize us: http://vi.sualize.us/carbon_chirality_laszlo_peter_biro_chirality_nanotube_fullerene_picture_ja2R.html

[11] *Carbon Nanotubes: Optical Properties Part 1 (Nanotechnology)*. (n.d.). Retrieved July 28, 2013, from what-when-how: http://what-when-how.com/nanoscience-and-nanotechnology/carbon-nanotubes-optical-properties-part-1-nanotechnology/

[12] Popov, V. N. (2004). Carbon nanotubes: properties and application. *Materials Science and Engineering, 43*, 61-102.

[13] Xavier Blase, M. D. (n.d.). *Electronic Properties of Carbon Nanotubes*. Retrieved July 28, 2013, from http://sites.uclouvain.be/pcpm/themes/ELECTRONIC_NT.php

[14] M.S. Dresselhaus, G. D. (n.d.). *Carbon Nanotubes.* New York: Springer.

[15] Guiru Gu, Y. L.-S. (2011). All-Printed Thin-Film Transistor Based on Purified Single-Walled Carbon Nanotubes with Linear Response. *Journal of Nanotechnology, 2011*.

[16] I. Hamberg, C. G. (1986). Evaporated Sn-doped In2O3 films: Basic optical properties and applications to energy-efficient windows. *Journal of Applied Physics, 60*(11).

[17] H. Kataura, Y. K. (1999). Optical Properties of Single-Wall Carbon Nanotubes. *Synthetic Metals, 103*, 2555-2558.

[18] Sevillano, J. G. (n.d.). *Structure and mecanical properties of Carbon nanotubes*. Retrieved July 28, 2013, from TECNUN: http://www.tecnun.es/asignaturas/estcompmec/documentos/carbnanotu.pdf

[19] M.F. Yu, O. Lourie, M.J. Dyer, K. Moloni, T.F. Kelly, R.S. Ruoff, Strength and breaking mechanism of multi-walled carbon nanotubes under tensile load, Science 287 (2000) 637.

[20] E.W. Wong, P.E. Sheehan, C.M. Lieber, Nanobeam mechanics: elasticity, strength and toughness of nanorods and nanotubes, Science 277 (1997) 1971.

[21] *Carbon Nanotubes, Production Methods for Carbon Nanotubes Including Arc Discharge, Laser, Chemical Vapor Depsition and Ball Milling by Cheap Tubes Inc*. (2006, May 16). Retrieved July 28, 2013, from Azonano: http://www.azonano.com/article.aspx?ArticleID=1561

[22] P. L. Walker Jr., J. F. (1959). Carbon Formation from Carbon Monoxide-Hydrogen Mixtures over Iron Catalysts.I. Properties of Carbon Formed. *Journal of Physical Chemistry, 63*(2), 133-140.

[23] M. José-Yacamán, M. M.-Y. (1993). Catalytic growth of carbon microtubules with fullerene structure. *Applied Physics Letters, 62*, 202-204.

[24] Kannan Balasubramanian, M. B. (2005). Chemically Functionalized Carbon Nanotubes. *small, 1*(2), 180-192.

[25] Quigley, M. (2012). *Rapid Laser Scanning Based Surface Texturing for Energy Applications.* Masters Thesis, Stony Brook University, Mechanical Engineering.

[26] *COOH Functionalized Carbon Nanotube Suspensions*. (n.d.). Retrieved July 28, 2013, from NanoLab: http://www.nano-lab.com/nanotubesuspensions.html

[27] Patel, P. (2009, January 23). *Clear Carbon-Nanotube Films*. Retrieved July 28, 2013, from Technology Review: http://www.technologyreview.com/news/411751/clear-carbon-nanotube-films/

[28] *MARUBENI INFORMATION SYSTEMS CO., LTD.* (n.d.). Retrieved July 28, 2013, from Battery Japan: https://www.r-expo.jp/mar2011/exhiSearch/BJ/en/search_detail.php?id=1542

[29] Zhiping Luo, A. O.-B. (2011). Thermal stability of functionalized carbon nanotubes studied by in situ transmission electron microscopy. *Chemical Physics Letters, 513*(1-3), 88-93.

[30] Georgakilas V, V. D. (2002). Purification of HiPCO Carbon Nanotubes via Organic Functionalization. *Journal of the Americal Chemical Society, 124*(48), 14318-14319.

[31] Liangbing Hu, D. S. (2009). Infrared transparent carbon nanotube thin films. *Applied Physics Letters, 94*(8).

[32] T. W. EBBESEN, H. J. (1996). Electrical conductivity of individual carbon nanotubes. *Nature, 382,* 54-56.

[33] Z. C. Wu, Z. H. (2004). Transparent, Conductive Carbon Nanotube Films. *Science, 305*, 1273-1276.

[34] Weeks, C. (2006). Flexible carbon nanotube transparent electrodes. *Flexible Substrate*, 40-43.

[35] Yao Zhao, J. W. (2011). Iodine doped carbon nanotube cables exceeding specific electrical conductivity of metals. *Scientific Reports, 1*(83).

[36] Luiz F. C. Pereira, C. G. (2009). Upper bound for the conductivity of nanotube networks. *Applied Physics Letters, 95*(3).

[37] High conductivity transparent carbon nanotube films deposited from superacid. (2011). *Nanotechnology, 22*(7).

[38] B. Ruzicka, L. D.-N.-P. (2000). Optical and dc conductivity study of potassium-doped single-walled carbon nanotube films. *Physical Review B, 61*(4), 2468-2471.

[39] Yu, E.T., and J. van de Lagemaat. "Photon management for photovoltaics." MRS BULLETIN. 36. (2011): 424-428.

[40] P. T. Araujo, I. O. (2008). Nature of the constant factor in the relation between radial breathing mode frequency and tube diameter for single-wall carbon nanotubes. *Physical Review B, 77*(24).

[41] Amer, M.S., M.A. El-Ashry, L.R. Dosser, K.E. Hix, J.F. Maguire, and Bryan Irwin. “Femtosecond versus nanosecond laser machining: comparison of induced stresses and structural changes in silicon wafers." ELSEVIER. (2004): 162-167.

[42] Paschotta, Rudiger, ed. *Encyclopedia of Laser Physics and Technology*. s.v. "Resonator Modes." http://www.rp-photonics.com/resonator_modes.html (accessed March 8, 2012).

[43] Sher, Meng-Ju, Mark Winkler, and Eric Mazur. "Pulsed-laser hyperdoping and surface texturing for photovoltaics." MRS BULLETIN. 36. (2011): 439-445.